Distribution Agreement

In presenting this thesis as a partial fulfillment of the requirements for an advanced degree from Emory University, I hereby grant to Emory University and its agents the non-exclusive license to archive, make accessible, and display my thesis in whole or in part in all forms of medial, now or hereafter known, including display on the world wild web. I understand that I may select some access restrictions as part of the online submission of this thesis. I retain all ownership rights to the copyright of the thesis. I also retain the right to use in future works (such as articles or books) all or part of this thesis.

Signature

_____ _____

Yutao Yang Date

Paclitaxel and Cyclostreptin in the Tubulin Binding Site

By

Yutao Yang

Master of Science

Chemistry

_____
Dennis C. Liotta
Advisor

_____
James P. Snyder
Advisor

_____
David Lynn
Committee Member

_____
Tianquan Lian
Committee Member

Accepted:

_____
Lisa A. Tedesco, Ph.D.
Dean of the Graduate School

_____
Date

Paclitaxel and Cyclostreptin in the Tubulin Binding Site

By

Yutao Yang

B.S., University of Science and Technology of China, 2006

Advisor:
Dr. Dennis C. Liotta
Dr. James P. Snyder

An abstract of
A thesis submitted to the Faculty of the Graduate School of Emory University
in partial fulfillment of the requirements for the degree of
Master of Science
in Chemistry
2008

Abstract

Paclitaxel and Cyclostreptin in the Tubulin Binding Site

By Yutao Yang

The development of new anti-cancer drugs is important in these days. In the first two parts, two microtubule stabilizing agents were explored. In part 1 of this thesis, two conformers of paclitaxel, a FDA approved drug, were compared. In part 2, cyclostreptin was explored using different docking algorithms. In the third part, a high potency measles virus inhibitor was explored by searching the protein data bank.

Paclitaxel and Cyclostreptin in the Tubulin Binding Site

By

Yutao Yang

B.S., University of Science and Technology of China, 2006

Advisor:
Dr. Dennis C. Liotta
Dr. James P. Snyder

A thesis submitted to the Faculty of the Graduate School of Emory University
in partial fulfillment of the requirements for the degree of
Master of Science
in Chemistry
2008

Acknowledgments

The work has been done under supervision of Dr. Dennis C. Liotta and Dr. James P. Snyder. I am likewise grateful to the people in the molecular modeling lab, chemistry department, Emory University for many helpful discussions. Dr. David Lynn and Dr. Tianquan Lian are greatly appreciated for their constant support of my efforts.

Table of Contents

List of Tables

List of Figures

Part 1. Tubulin bounded PTX conformation: T-Taxol or PTX-NY

Introduction

Cancer represents one of the most severe health problems worldwide, and the development of new anticancer drugs is a field of utmost importance in drug discovery. A renowned and important target for anticancer drugs among many other molecular targets is the mitotic spindle[2]. It works by incorporating and removing αβ-tubulin heterodimers from microtubule ends. Microtubule inhibitors are an important group of anticancer agents that interfere with microtubules within the mitotic spindle of rapidly dividing cells. There are two distinct groups of microtubule inhibitors[3]: one inhibits the assembly of tubulin heterodimers into microtubule polymers, the other one stabilizes microtubules under normally destabilizing conditions and promotes the assembly of tubulin heterodimers into microtubules. The latter microtubule-stabilizing agents (MSAs) are best represented by the blockbuster drug, paclitaxel (PTX, **Figure 1-1**)[4,5].

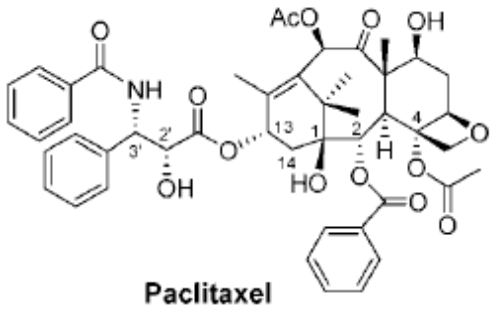

Figure 1-1. Paclitaxel (PTX) structure

The molecule, PTX originating from the bark and leaves of the Yew tree, was discovered to be a potent anti-cancer candidate in a natural product screening program as early as 1967[6]. In 1992, 25 years after discovery, FDA approved PTX for treatment of late stage ovarian and breast cancer[7]. Though the 3D structure of PTX was discovered in1995[8], investigation of different bioactive conformations of PTX led to the discovery of novel anticancer drugs with higher activity[9].

Nogales and coworkers reported the first attempt to determine the PTX structure in tubulin in 1998[10]. The Electron Crystallographic (EC) structure of the PTX bound, Zn^{2+} stabilized tubulin dimer was reported at 3.7Å resolution (1TUB), proving a low-resolution picture of the PTX conformation and its corresponding binding site. In 2001, the 1TUB structure was further refined to 3.5Å resolution known as the 1JFF structure[11]. At the meantime, a computational study of the PTX structure on tubulin was also reported[12]. The first proposed tubulin-bound PTX structure was a "T-Taxol" conformation[12]. Since in the T-taxol conformation a short distance between the C-4 group and the C-3' phenyl ring was found, a series of macrocyclic taxanes with a C-4 and C-3' linker in the conformations were introduced to rigidify the T-Taxol conformation and examine the bioactivity of the T-taxol conformation. These T-Taxol analogs remained in the T like conformation throughout different experiment and exhibited higher bioactivity than the original PTX in both cytotoxicity and tubulin-polymerization assays[13-14].

However, Ojima's group proposed their own PTX conformation in 2005[15]. They believed that their model has stronger PTX-tubulin interactions than T-Taxol. In their model the key difference compared to the T-Taxol is the orientation of the C2'-OH group within the C-13 side chain. Ojima's group proposed a hydrogen bond between the C2'-

OH group and His227 in tubulin in their computational model, while this C2'-OH group in T-Taxol with a different spatial orientation does not form this hydrogen bond. At the same time, their model also meets the two C13-F19 distances of 2-(4-fluorobenzoly) PTX by the REDOR NMR study[14,16], which were reported to be two key parameters that the tubulin-PTX conformation should meet. Thus, Ojima's group named their conformation "REDOR-Taxol". However, not only does the T-Taxol conformation meet these criteria, there are also many other PTX conformations that do so. Emory's T-Taxol conformation and all of the latter can also be called REDOR-Taxol. In order to clarify, we will use PTX-NY instead to refer to Ojima's so-called "REDOR-Taxol" conformation in this thesis.

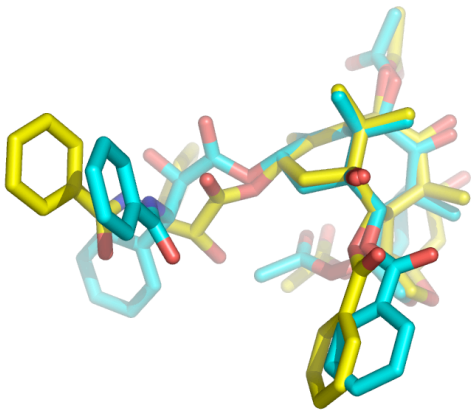

Figure 1-2. Superposition of PTX-NY (Yellow) and T-Taxol (Cyan)

Early works showed that the T-Taxol C-13 side chain fits experimental density very well, while PTX-NY cannot fit into the tubulin binding site by experimental data[14,17,18]. In my work, I would like to compare these two conformations to see which one is more stable using a variety of molecular mechanics and quantum chemistry methods. Likewise

I will describe a study to examine which one is able to fit better in the tubulin binding site by a protein-ligand docking comparison. A molecular dynamics comparison was also performed to compare these two conformers' dynamic properties.

Methods and Results

C-13 side chain conformational analysis

The T-Taxol and PTX-NY C-13 side chains were found to be the main difference between these two conformations. Thus, the C-13 side chain was extracted from the full taxane structure, and a methyl group was added to the C-13 carbon. The structure of the C-13 side chain utilized in the calculations is indicated in **Fig1-3**. Two different side chain conformers were optimized with both MMFFs and OPLS-2005 force fields in Maestro 8.5.111[19] with all the torsion angles restrained to their original values.

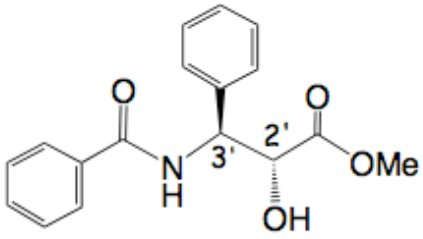

Figure 1-3. The C-13 side chain structure

Force Field	T-Taxol, kJ/mol	PTX-NY, kJ/mol	ΔE, kcal/mol
MMFFs	253.3	233.8	4.7
OPLS-2005	-36.7	-69.1	7.8

Table 1. Relative molecular mechanics energies from MMFFs and OPLS-2005 geometry optimized T-Taxol and PTX-NY C-13 side chains with all the torsion angles constrained

To determine if both T-Taxol and PTX-NY C-13 side chain conformers are energy minima on the both MMFFs and OPLS-2005 molecular mechanics energy surfaces, conformational searches were performed using both MMFFs and OPLS-2005 force fields with the mixed Monte Carlo and Low Mode methods in Maestro 8.5.111[20]. 10,000 step conformational searches were performed; the global minima were found 200 and 28 times, respectively[21]. The resulting structures were further optimized to convergence, and 102 and 101 unique conformations were retained, respectively. A 3-D shape-based searching tool, ROCS[22,23], was used to locate structure in the conformational pool. The MMFFs and OPLS-2005 optimized structures were used as templates, respectively, and the conformations from the conformational search were used as conformational pools. The T-Taxol side chain proved to be 7.7 kcal/mol above the global minima using MMFFs force field and 1.6 kcal/mol above the global minima using OPLS-2005 force field, while PTX-NY side chain was found 27.2 and 35.0 kcal/mol above the same global minima, respectively.

The OPLS-2005 constrained-optimized structures of both PTX-NY and T-Taxol side chains were imported into Gaussian03[24], and single point calculations were performed using HF (with basis sets 6-31G*, 6-311G* and 6-311+G*), B3LYP (6-31G*, 6-311G* and 6-311+G*) and MP2 (6-31G*, 6-311G* and 6-311+G*) methods. The resulting energies and differences are provided in **Table 2**

Method/Basis set	PTX-NY, a.u.	T-Taxol, a.u.	E(NY)-E(T),[a] a.u.	E(NY)-E(T),[a] kcal/mol
HF/6-31G*	-1007.558830	-1007.573941	0.015111	9.5
HF/6-311G*	-1007.762566	-1007.778154	0.015587	9.8
HF/6-311+G*	-1007.780290	-1007.795612	0.015321	9.6
B3LYP/6-31G*	-1013.686174	-1013.699795	0.013621	8.5
B3LYP/6-311G*	-1013.924903	-1013.939159	0.014255	8.9
B3LYP/6-311+G*	-1013.946069	-1013.959463	0.013394	8.4
MP2/6-31G*	-1007.558872	-1007.573967	0.015094	9.5
MP2/6-311G*	-1007.762580	-1007.778172	0.015592	9.8
MP2/6-311+G*	-1007.780290	-1007.795614	0.015323	9.6

Table 2. Single point quantum chemical calculations on the OPLS-2005 optimized T-Taxol and PTX-NY C-13 side chains (all torsions constrained) using different methods and basis sets. [a] NY = PTX-NY and T = T-Taxol conformations.

Energy comparisons for full T-Taxol and PTX-NY structures

Both T-Taxol and PTX-NY were optimized with all the torsions constrained using the following force fields: MM2, MMFFs, OPLS-2001, OPLS-2005 and OPLS-2005/MMFFs. Then, the structures of T-Taxol and PTX-NY were optimized without constraints using the same set of force fields. The relative energies are provided in **Tables 3 and 4**, respectively.

Force Field	PTX-NY, kJ/mol	T-Taxol, kJ/mol	ΔE, kJ/mol	ΔE, kcal/mol
MM2	543.6	508.4	35.2	8.4
MMFFs	936.3	891.0	45.3	10.8
OPLS-2001	275.8	223.8	52.0	12.4
OPLS-2005	135.2	74.4	60.8	14.5
OPLS-2005/MMFFs [a]	937.2	894.4	42.8	10.2

Table 3. T-Taxol and PTX-NY structures optimized using several molecular mechanics methods with all the torsion angles constrained.

[a] Constraint optimization first using MMFFs, then using OPLS-2005.

Force Field	PTX-NY, kJ/mol	T-Taxol, kJ/mol	ΔE, kJ/mol	ΔE, kcal/mol
MM2	496.6	485.5	11.1	2.7
MMFFs	901.2	867.0	34.2	8.2
OPLS-2001	220.6	207.3	13.3	3.2
OPLS-2005	73.8	52.8	21.0	5.0

Table 4. T-Taxol and PTX-NY conformations optimized without constraints using several molecular mechanics methods.

T-Taxol and PTX-NY geometries obtained from torsion-constrained optimization with the OPLS-2005 followed by MMFFs force fields were imported into Gaussian03. Single point energies using several different Gaussian models were calculated for these two geometries. The results are listed in **Table 5**.

Model	PTX-NY, a.u.	T-Taxol, a.u.	E(NY)-E(T),[a] a.u.	E(NY)-E(T),[a] kcal/mol
B3LYP/6-31G*	-2929.501663	-2929.527763	0.026100	16.4
B3LYP/6-311G*	-2930.188739	-2930.213795	0.025057	15.7
B3LYP/6-311+G*	-2930.238158	-2930.263956	0.025798	16.2

Table 5. Single point quantum chemical energies for T-Taxol and PTX-NY conformations, produced by optimizations with OPLS-2005 followed by MMFFs with all torsion angles fixed to these conformations

[a] NY = PTX-NY and T = T-Taxol conformations.

Bridged taxanes K1 and K2

The structures of **NY-K1** and **NY-K2** were produced by directly introducing the linker into the PTX-NY docked in the tubulin[25] using Maestro8.5.111. Then these structures were energy-minimized using the OPLS_2005 force field, the distance-dependent electrostatic treatment and the GBSA/H2O continuum solvation model. The backbone of the protein was fixed throughout the energy minimization. After the optimization, the NY-K1 and NY-K2 structures were extracted from the proteins, respectively.

Structures of **T-K1** and **T-K2** in T-Taxol conformations were from a previously reported molecular dynamics (MD) study[26]. K1 and K2 structures are illustrated in **Figure 1-4**

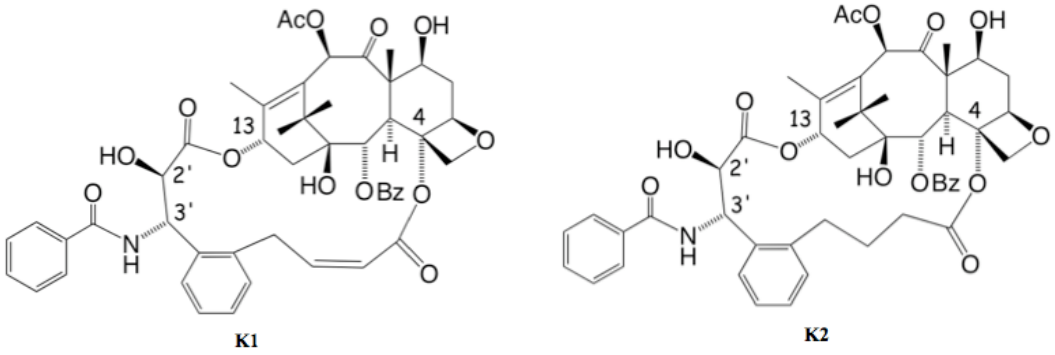

Figure 1-4. K1 and K2 structures

The bridged conformers were energy-minimized using a variety of force fields and force field combinations without constraints. All of the bridged structures stayed in their original conformations during these optimizations. The results are listed in **Tables 6** and **7**.

Force Field	T-K1, kJ/mol	NY-K1, kJ/mol	ΔE, kJ/mol	ΔE, kcal/mol
MM3	787.8	816.8	29	6.9
MMFFs	988.5	1036.2	47.7	11.4
OPLS-2005	85.2	204.0	118.8	28.4
OPLS-2005/MM3[a]	752.5	815.8	63.3	15.1
OPLS-2005/MMFFs[b]	945.6	1031.9	86.3	20.6

Table 6. T-K1 and NY-K2 geometry optimized without constraints using several different force fields

[a] Optimized with OPLS-2005 followed by MM3

[b] Optimized with OPLS-2005 followed by MMFFs

Force Field	T-K2, kJ/mol	NY-K2, kJ/mol	ΔE/(kJ/mol)	ΔE/(kcal/mol)
MM3	711.3	753.6	42.3	10.1
MMFFs	914.2	944.9	30.7	7.3
OPLS-2005	72.7	112.5	39.8	9.5
OPLS-2005/MM3 [a]	712.4	748.7	36.3	8.7
OPLS-2005/MMFFs [b]	914.6	939.1	24.5	5.9

Table 7. T-K2 and NY-K2 geometry optimized without constraints using several different force fields

[a] Optimized with OPLS-2005 followed by MM3

[b] Optimized with OPLS-2005 followed by MMFFs

The optimized conformations of NY-K1, NY-K2, T-K1, and T-K2 using OPLS_2005 force field followed by MMFFs force field were imported to Gaussian03 to be further explored. Single point calculations using semi empirical B3LYP method and 6-31G* basis were performed on all four conformations, the relative energies are listed in **Table 8.**

	T-Taxol, a.u.	PTX-NY, a.u.	E(NY)-E(T),[a] a.u.	E(NY)-E(T),[a] kcal/mol
K1	-3005.716643	-3005.672321	0.044321	28.3
K2	-3006.934127	-3006.944942	0.010815	6.8

Table 8. Single point B3LYP/6-31G* quantum chemical energies for K1 and K2 in T-Taxol and PTX-NY conformations optimized with OPLS-2005/MMFFs

[a]NY = PTX-NY and T = T-Taxol conformations;

Molecular dynamics (MD) for T-Taxol and PTX-NY in water

For PTX, the polar conformation was solvated in a box of 512 SPC water molecules and subjected to 11 ns of molecular dynamics calculation at 300 K with a time step of 1 fs under NPT conditions in GROMACS 3.2.1[27,28]. Examination of the MD trajectory by comparing the overall RMSD for PTX relative to T-Taxol over the 11 ns time course of the simulation revealed that, while the molecule assumes many different conformations, the T-form is sampled at least four times. In the present work, a similar analysis was performed for PTX-NY. The PTX-NY conformation did not appear among the structures.

Docking of T-Taxol and PTX-NY in β-tubulin.

The PTX ligand in ß-tubulin (pdb code 1JFF[11]) was removed, and an extra precision flexible ligand Glide[1,29] docking (Maestro 8.5.111) was performed using T-Taxol, PTX-NY and two X-ray structures A (extended) and B (polar)[30]. All of the four docking results showed that the most favorable poses place T-Taxol into the PTX binding site. No PTX-NY was found in all of the four docking poses.

Extra precision induced-fit docking with Prime[31] in Maestro 8.5.111 explores flexibility of both the ligand and the protein in the target region of the selected protein. The protocol was utilized to compare any possible reorganization of the binding site that might better accommodate the PTX-NY conformation. However, the T-Taxol docks with very little reorganization of protein side chains to deliver the T-Taxol bound conformation once again. The PTX-NY turned out to be T-Taxol after the induced fit

docking again illustrates that T-Taxol accommodate better in the binding sites than the PTX-NY conformation.

Discussion

Relative energies for PTX C-13 side chains

The main difference between T-Taxol and PTX-NY occurs in the C-13 side chain. There is no big difference in other parts of the molecule. We would like to gain some general stability information of these two PTX conformations by comparing the relative energies of the C-13 side chain using different methods.

We first constrained all of the C-13 side chain torsions, and let the bond lengths and bond angles relax using two most popular molecular mechanics force fields, which are MMFFs and OPLS-2005. The PTX-NY conformation is 5 kcal/mol less stable than the T-Taxol conformation with the MMFFs force field and is 8 kcal/mol less stable with the OPLS-2005 force field.

To compare the relative energies of molecular mechanics optimized conformations using quantum chemistry methods, we imported these MMFFs and OPLS-2005 optimized conformations into Gaussian03, and a variety of methods and basis sets including polarization and diffusion were used to evaluate the relative energies of these two optimized conformations. From all of these calculations, PTX-NY conformer was less stable by 8-10 kcal/mol compared to the T-Taxol conformer.

To ensure that the MMFFs and OPLS-2005 optimized structures are local minima on their energy surfaces, 10,000 step conformational searches were performed with the two

force fields to locate the energy minima, which are MMFFs and OPLS-2005. The number of global minima returned by conformational search using MMFFs and OPLS-2005, respectively, indicated the search is complete. Then, ROCS 3D searches were used to locate PTX-NY and T-Taxol side chain conformers in the conformational pool. The result showed again that T-Taxol side chain more resembles the global minimum and is more energetically stable than PTX-NY side chain. The difference of energy between PTX-NY and T-taxol is about 20-30 kcal/mol from conformational and ROCS searches.

In this point, the C-13 side chain alone shows that T-Taxol is more stable compared to PTX-NY by 10 kcal/mol using the more precise quantum chemistry calculations. This 10 kcal/mol difference is large, which cannot be compensated by a single hydrogen bond with the tubulin backbone. However, this is only the comparison on C-13 side chain. There might be some other interactions on other part of the molecule we might have neglected by only exploring the C-13 side chain, thus we need to compare the full PTX conformations between PTX-NY and T-Taxol in the next step to see if the energy difference follow the same pattern as for the C-13 side chain alone.

Relative energies for full PTX conformations

First of all, the full PTX-NY and T-Taxol conformers were optimized using different force fields with all the torsions fixed. With this treatment, the bond lengths and bond angles were relaxed according to the force fields and the conformers remained in their published conformations[12,15]. All of the force field optimization results reveal that T-Taxol is 8-15 kcal/mol more stable than PTX-NY, which is exactly what we have observed in the side chain calculations.

Single point quantum chemistry calculations were also applied to the optimized conformations of both PTX-NY and T-Taxol with all torsions fixed. The result again showed T-Taxol to be more stable than PTX-NY by about 16 kcal/mol. (**Table 5**)

Until this point, we still worked on the conformations with all the torsions fixed; we would like to explore what will happen if the torsion constraints were removed. Will the PTX-NY and T-Taxol conformers stay in their original conformations? What's the energy difference between these two conformers after removing all constrains? Four force fields or force field combinations are used as listed in **Table 4**. The results again point out that T-Taxol is more energetically stable than PTX-NY by 3-8 kcal/mol without constraints. By looking into these optimized conformers, PTX-NY and T-Taxol retained their original conformations after optimizations using different force fields.

The full PTX calculations all reveal that T-Taxol is a more energetically favored conformation compared to PTX-NY, and also show that the C-13 side chain is a reasonable computational substitution to explore the differences between T-Taxol and PTX-NY, since the energy difference between T-Taxol side chain and PTX-NY side chain is similar to the difference between the full structure conformers.

Highly active bridged taxanes

There have been many attempts to modify the PTX structure, hoping to find other more potent any cancer drugs. Among these attempts, one of these ideas is to introduce a linker into the PTX molecule, locking the molecular conformation in order to keep the bioactivity. Two macrocyclic taxoids were shown to be more cytotoxic and more active in tubulin polymerization[13,26,32] than PTX (**Fig1-3).** Both of these two structures have a linker

between the C-4 acetate group and the C-3' phenyl group. According to previous work, the T-K1 and T-K2 conformers docked into PTX binding site on tubulin very well.

Both K1 and K2 can adopt the T-Taxol conformation and the PTX-NY conformation. To compare the stability of PTX-NY and T-Taxol, the macrocyclic conformers, which can rigidify the PTX conformations, especially the C-13 side chain conformations, also need to be explored.

PTX-NY K1 and K2 conformations were generated by methods the Ojima's group adopted. T-Taxol K1 and K2 conformations are directly from the previously published T-Taxol form[13,26,32]. Since these macrocyclic conformers are more rigid in the C-13 side chain, we optimized them without constraining the torsions. Different force fields listed in **Table 6** and **Table 7** were used. The results again reveal that the T-Taxol conformer geometry is at least 7 kcal/mol more stable in K1 and 6 kcal/mol more stable in K2 compared to PTX-NY conformer. Again to compare the relative energies by quantum chemistry methods, selected force field optimized structures were imported into Gaussian03 to perform single point energy calculations. (**Table 8**) The single point calculations also show that T-K1 is 28 kcal/mol more stable than NY-K1 and T-K2 is 7 kcal/mol more stable than NY-K2, which is consistent with all the previous calculations.

As a result, the macrocyclic PTX analogs provide another piece of evidence that the T-Taxol conformer is more stable than the PTX-NY conformer. Especially the K1 conformer increases the energy difference between T-Taxol and PTX-NY compared to the original PTX molecules by about 20 kcal/mol.

Conformational differences between T-Taxol and PTX-NY

Previous energetic comparisons all favored the T-Taxol conformation relative to the PTX-NY conformation. By superimposing T-Taxol and PTX-NY (**Figure 1-2**), we found that the main difference between them occurs in the C-13 side chain. In the T-Taxol conformation, the C1'-OH group and the C2'=O group are on the same side by looking from C2' to C1'. In **Figure 1-5** we can see clearly that there's a hydrogen bond between the hydrogen on C1'-OH and the oxygen on C2'=O, this kind of hydrogen bond typically offers 5 kcal/mol more stable energy.

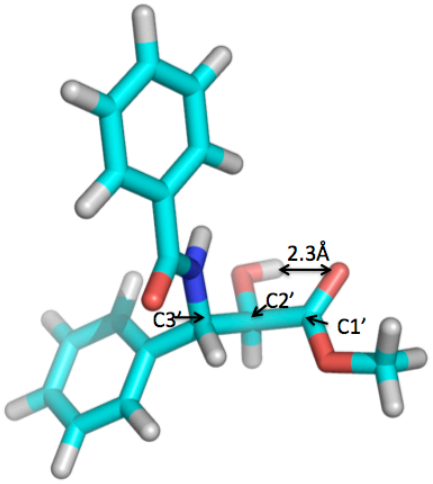

Figure 1-5. T-Taxol side chain conformer

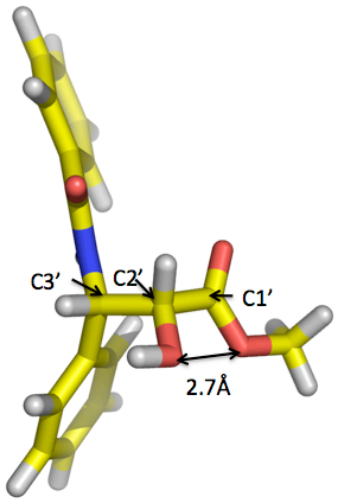

Figure 1-6. PTX-NY side chain conformer

At the meantime, the PTX-NY conformer (**Figure 1-6**) not only lacks the hydrogen bond, which exists in the T-Taxol conformer; it also incorporates a repulsive interaction. In the PTX-NY conformation, the distance between the oxygen from the C2'-OH group and the ester oxygen connected to C1' is 2.7 Å, which is 0.3 Å less than the sum of the van de Waals radii of two oxygens[33]. This short contact between these two oxygens leads PTX-NY to be less stable.

The hydrogen bond in the T-Taxol conformer together with the oxygen-oxygen repulsion in the PTX-NY conformer creates the energy difference between the T-Taxol and the PTX-NY conformers. There may also be other structural reasons that induce the energy difference between these two conformers.

Molecular dynamics of PTX in water to locate the T-Taxol and PTX-NY conformations

Up to this point, different calculations using molecular mechanics and quantum chemistry were exploited to study conformational energy differences. All of these efforts

reveal that T-Taxol is more stable than PTX-NY by about 10 kcal/mol. In order to explore the dynamic properties of PTX-NY and T-Taxol, different conformations of PTX were subject to molecular dynamics calculations in a box of water molecules (see Methods and Results). In the calculation, we use a box of water instead of vacuum, which provides the PTX molecule with a polar environment to mimic the tubulin binding site. In Ojima's model, they suggested that PTX-NY has a hydrogen bond between C2'-OH and the tubulin His227[15]. A box of water can hold this kind of hydrogen bonds if there are any and eventually stabilize the conformation of PTX-NY.

A polar conformation of PTX was used as a starting point in the 11ns MD calculation. By analysis of the RMSD together with the molecular conformations during the MD trajectory, we found T-Taxol conformation at least 4 times. At the same time, we did not see any of PTX-NY conformation presented in the 11ns MD trajectory, which implies that the hydrogen bond between C2'-OH group and tubulin His229 group is insufficient to compensate the energy difference between T-Taxol and PTX-NY during a molecular dynamic calculation.

The fact that the T-Taxol conformation only presented 4 times during the MD trajectory did not mean that T-Taxol is not a stable conformation. The present of water solutions is not an ideal mimic of the tubulin binding site, thus the T-Taxol conformation may change a little bit to accommodate the water solution environment instead of keeping in T-Taxol conformation like in the tubulin binding site.

ß-Tubulin binding poses for T-Taxol and PTX-NY conformations

So far we have only compared the stability of T-Taxol and PTX-NY under vacuum or water solution environment, we haven't explored how these two conformations will dock into the tubulin binding site. Will PTX-NY fit the tubulin binding site better than T-Taxol? In order to answer this question, a set of docking calculations was performed.

The electron crystallographic protein 1JFF[11] was employed to provide a grid box for different conformations of PTX to dock into. Four different PTX conformations (the T-Taxol, the PTX-NY, the X-ray A conformation and the X-ray B conformation, see methods for detail) were docked into the grid box using the extra precision docking algorithm. In all of the four docking results, T-Taxol conformation was returned as the top scored poses. A more impressive discovery is that almost all of the returned poses are in T-Taxol conformation from all of the four PTX docking results, and PTX-NY does not appear a single time in these results.

By the Glide docking, we can conclude that the T-Taxol conformation fits the tubulin binding site in 1JFF better than the PTX-NY conformation. However, the protein may be subject to reorganization upon ligand binding. For this reason, we would like to explore what will happen if we also allow the protein backbone and side chain close to the binding site to be flexible together with the ligand. Induced Fit Docking, a sequential combination of Glide[1,29] Docking, Prime[31] protein refinement and Glide Redocking, was an appropriate procedure to allow both the ligand and the protein to be flexible. The Induced Fit Docking again led to the same result: even we allow the protein to move around the binding site, only T-Taxol is found in the binding pocket, and none of returned poses puts PTX-NY in the binding area.

Both the Glide docking and Induced Fit Docking implies that only the T-Taxol conformation can accommodate the PTX binding site in the 1JFF structure. The PTX-NY conformation cannot fit into the PTX binding pocket in the 1JFF model, even when the proteins allowed to have some flexibility. In order to accommodate PTX-NY in the binding site, the binding pocket must rearrange, which is inconsistent with the crystal structure we've determined by now.

Summary and Conclusions

The T-Taxol conformation was first observed for PTX in experiment in 2000[34] and was later proved to fit the density in two independent crystallographic analyses[11,12]. Ojima's group also proposed the PTX-NY conformation, which fits only the data of REDOR experiment. However, in our experiments, we compared T-Taxol and PTX-NY conformations using a variety of methods, all of the results show that the T-Taxol conformation is a more energetically stable conformation.

Molecular mechanics and quantum chemistry comparison were first performed to the C-13 side chain, the parent PTX and the macrocyclic analogy K1 and K2 for both PTX-NY and T-Taxol. All of these results support that the T-Taxol conformation is a more energetically stabilized conformation compared to the PTX-NY conformation by 3-28 kcal/mol (**Table 1-8**)

The next evaluation is an 11ns molecular dynamics trajectory analysis for PTX in a box of water at 300K. In the molecular dynamics trajectory, T-Taxol presented several times along the molecular dynamics path, while no PTX-NY conformation was detected.

This again confirmed that PTX-NY is less stable in our molecular dynamics environment compared to T-Taxol.

Docking with both rigid protein and flexible protein were also performed. The T-Taxol docked perfectly in the tubulin binding site, while PTX-NY never docked into the PTX pocket in all of these docking calculations we performed.

Ojima's group has just published a paper about a new macrocyclic PTX[35], which they claim is in the PTX-NY form. However, by superimposing their 9b X-ray structure with T-Taxol, we found that their new macrocyclic PTX analogy is in the T-Taxol conformation, and this conformation is also more stable compared to the PTX-NY conformation.

Part 2. Docking and Reactivity of Cyclostreptin with tubulin

Introduction:

Cancer represents one of the most severe health problems worldwide, and the development of new anticancer drugs is a field of utmost importance in drug discovery. A renowned and important target for anticancer drugs among many other molecular targets is the mitotic spindle[2]. It works by incorporating and removing αβ-tubulin heterodimers from microtubule ends.

Microtubule inhibitors are an established and important group of anticancer agents. By interfering with microtubules within the mitotic spindle of rapidly dividing cells, these agents arrest cells in mitosis and cause apoptosis. There are two distinct groups of microtubule inhibitors[3]: one inhibits the assembly of tubulin heterodimers into microtubule polymers (such as colchicine), the other one stabilizes microtubules under normally destabilizing conditions and promotes the assembly of tubulin heterodimers into microtubules. The latter microtubule-stabilizing agents (MSAs) are best represented by the blockbuster drug, paclitaxel[4,5].

The microtubule-stabilizing properties of paclitaxel (Taxol) were first recognized in 1979 by Susan Horwitz and coworkers[5]. In the following few years, paclitaxel and its derivatives were the only class of compounds known to act as microtubule stablizers. However, since 1995 a variety of other natural products from diverse sources have been established to share the taxanes' ability to inhibit the depolymerization of microtubules.

The most prominent representatives of this group include epothilones A and B[36], discodermolide[37], and more recently, cyclostreptin[38].

Cyclostreptin (FR182877) is a natural bacterial product. It was first discovered from fermentations of Streptomyces sp. no. 98855 by researchers at Fujisawa Pharmaceutical Co., Ltd., in Japan in 2000[38,39]. Early research revealed that cyclostreptin was a poor agent in stimulating tubulin assembly[40], though it potently inhibits paclitaxel binding to microtubules. Previous work proposed a mechanism for paclitaxel to approach its binding site, which is on the luminal side of microtubules. When paclitaxel approaches microtubules, a conformational change of the microtubule occurs, opening the pore in the microtubule wall, allowing paclitaxel to diffuse into the paclitaxel binding site[41]. This assumption disagrees somewhat with the fact that cyclostreptin strongly binds to microtubules, yet only weakly stimulates the tubulin assembly.

In trying to understand this paradox, Buey and coworkers[42] performed a set of experiments. Their conclusions were striking and have the potential to shed light on the development of a new class of MSAs. HPLC-MS experiments, kinetic experiments and cellular experiments were performed separately[42]. However, all of the results support the finding that cyclostreptin's potent cellular activity comes from the formation of an irreversible covalent bond with microtubules. Thus, cyclostreptin represents a new generation of MSAs, and this new class of MSAs had several advantages over the conventional ones. They are able to escape two important mechanisms of resistance: mutation of tubulin and ejection of drug from the cell by P-glycoprotein pumps.

By mass spectrometric analysis, the formation of covalent bonds between cyclostreptin and two amino acids on the microtubule, Thr220 and Asn228, was determined. Thr220 is found in a pore connecting the inside and outside of microtubules, whereas Asn228 is located in the interior of microtubules near both the paclitaxel and the GDP binding sites. Due to the paradoxical characteristic of cyclostreptin, which strongly binds to the microtubule, yet weakly stimulates the assembly of microtubule, and also due to a strict 1:1 cyclostreptin-β-tubulin stoichiometry, a new model was proposed. In this new model an initial low affinity binding site is located near the pore area on the outside of the microtubule. In addition, a new two-step mechanism for MSAs binding to microtubules was proposed based on this model. In the first step, MSAs bind to an outer, low-affinity site of microtubules, and MSAs then transfer through the pore into the inside of microtubules to bind to a high-affinity site in the lumen in the second step. This model explains why cyclostreptin binds to only 0.5–5% of the unassembled dimers. Also with cyclostreptin cross-linked to Thr220, the pore is blocked and other MSAs are unable to transfer through the pore to the internal paclitaxel binding site. Since the Asn228 site is also located near the GDP binding site, if the Asn228 attachment by cyclostreptin contributes to the drug's cytotoxic action, it is because of the possible displacement of GDP, which binds at a key location in the tubulin structure.

A mechanism in which a nucleophile in the microtubule pore region attacks cyclostreptin was proposed to explain the formation of the covalent bond. As **Figure 2-1** shows, it is a conjugate addition driven by releasing the strain in an unsaturated lactone in cyclostreptin. A set of experiments was performed to study of the reactivity of the

strained olefin of cyclostreptin[43], which revealed a relatively high reactivity with amine, thiol and other nucleophiles.

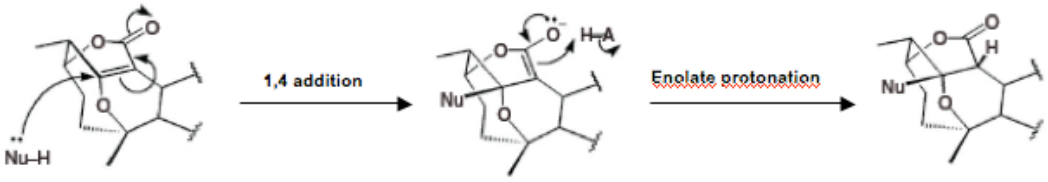

Figure 2-1. Mechanism for nucleophilic attack on cyclostreptin

Methods and Results

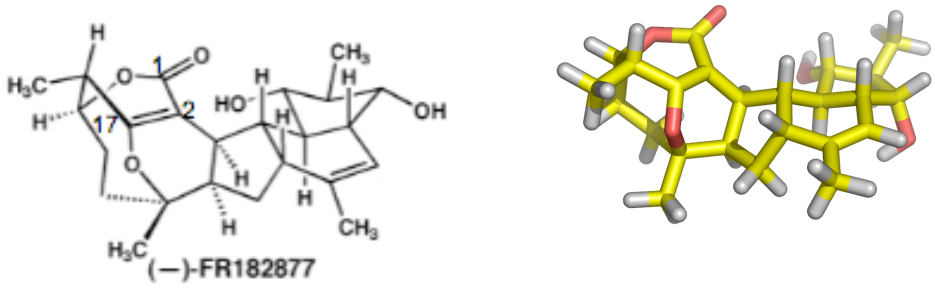

Figure 2-2: Structure of cyclostreptin. (a) Reference structure. (b) Structure built and optimized in Maestro8.0.308[1].

Since there is no 3-D structure of cyclostreptin, we started the project by constructing cyclostreptin in 3D using Maestro8.0.308[1] according to the topology presented by Christopher and coworkers[43]. A conformational search was performed to optimize and

obtain a reasonable geometry of cyclostreptin and to fix the hydrogens. The lowest energy conformation was selected as the ligand we used in dockings, which was shown in **Figure 2-2**.

AutoDock blind docking to the microtubule pore

The previously developed model of the type I microtubule pore[45] was used to perform a blind docking with the AutoDock4[44] package. Non-polar hydrogens were merged for both the microtubule pore and the cyclostreptin. A grid box was made to include the entire protein and a search grid was generated with AutoGrid4. Flexible ligand docking was performed in AutoDock4. Docking calculations were carried out using the Lamarckian genetic algorithm (LGA). We used initially a population of random individuals (population size: 150), a maximum number of 2,500,000 energy evaluations, a maximum number of generations of 27,000, a mutation rate of 0.02 and 50 outputs.

The blind docking covers several docking areas in the microtubule pore. After removing the poses at the edge of the pore, we found that there were three main areas in the tubulin that cyclostreptin is able to dock into: the paclitaxel (PTX) binding site (where Asp226 resides in), the GDP binding site (where Asn228 resides in), and the pore area (near Thr220). A cluster of docking poses is shown in **Figure 2-3**.

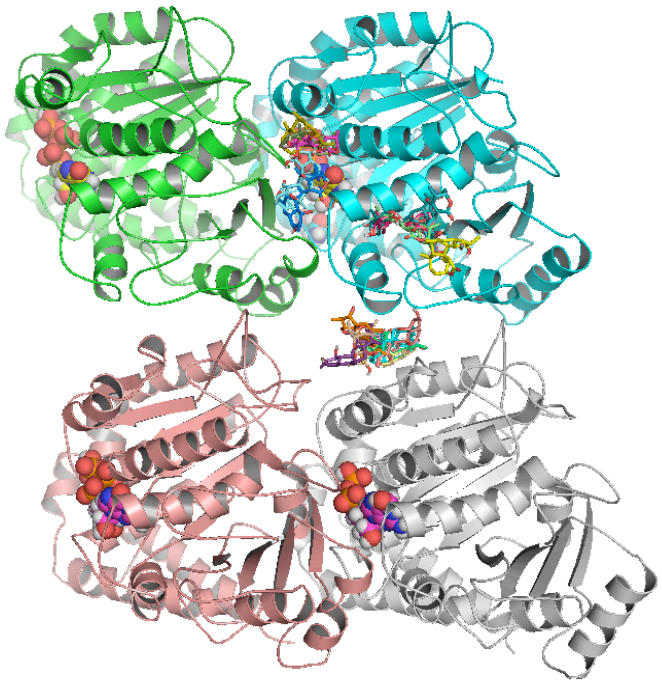

Figure 2-3. Cluster of docking poses from AutoDock Blind Docking. Look from the interior of the microtubule.

Glide flexible ligand docking

Glide docking[1,29] was performed in the following three areas, the paclitaxel binding site, the GDP binding site and the pore area. For the three binding sites, the receptor-grid files were generated using grid-receptor generation program in Maestro. Three different grid boxes of default size were generated at the centroid of the three active sites. The cyclostreptin ligand was docked within the three active sites using the "SP" Glide algorithm. To soften the potential for nonpolar parts, we performed a set of calculations using different van der Waals radii (from 0.80 to 0.25 Å).

A detailed analysis of the returned poses was performed by looking into the interactions between cyclostreptin and nucleophiles near the three docking areas,

especially interactions between nucleophiles on Thr220, Asp226, Asn228 and cyclostreptin (from our interpretation of the MS data). From the results, we found that cyclostreptin can be docked into the paclitaxel binding site, the pore area, but it cannot be accommodated at the GDP binding site. By measuring the distance between the nucleophilic atom on Thr220, Asn228, Asp226 and C2 on cyclostreptin respectively (**Figure 2-2**), we discovered that none of these distances are beyond 8 Å.

AutoDock docking with flexible residues

The same model of the type I microtubule pore was used to perform three independent flexible residues docking in the following three sites, the PTX binding site, the GDP binding site and the pore area. In the GDP binding site, we retained GDP in the site to mimic the natural protein. In the PTX binding site, a grid box was generated to exclude 12 key residues. The following docking allowed both the 12 residues and the ligand to be flexible. In the GDP binding site, 4 residues were made to be flexible. And in the pore area, there were 12 flexible residues. All of these three dockings employed the same algorithm and parameter as in the blind docking.

In the PTX binding site, we measured the following distances to see if Cys213, Asp226 or His229 can act as nucleophiles to interact with cyclostreptin.

(1). By measuring the distance between the C2 atom on cyclostreptin and the sulfur atom on Cys213, we discover that the nearest distance between them is 5.7 Å. In other poses, Cys213 are always far away from the C2 on cyclostreptin.

(2). The nearest distance between the C2 on cyclostreptin and the side chain oxygen on Asp226 is 3.6 Å, and this pose is captured in **Figure 2-4**. And there are also other poses that put Asp226 near C2 on cyclostreptin with distances less than 6 Å.

(3). None of the distances between C2 on cyclostreptin and the pyridine-like nitrogens on His229 are closer than 5 Å. However, a couple of poses have this distance between 5 Å and 6 Å. **Figure 2-5** captures a pose with a distance of 5.2 Å between the C2 on cyclostreptin and the pyridine-like nitrogen on His229.

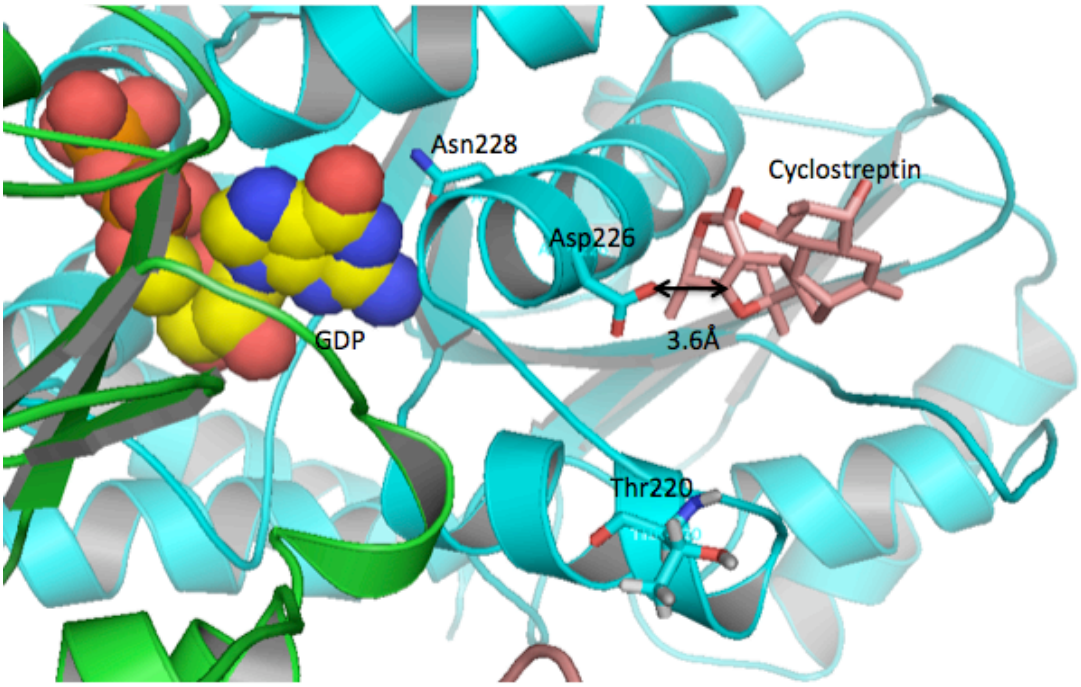

Figure 2-4. One of the docked poses in the PTX binding site using AutoDock4 flexible residue docking is illustrated. The distance between C2 on cyclostreptin and the side chain oxygen on Asp226 is 3.6 Å.

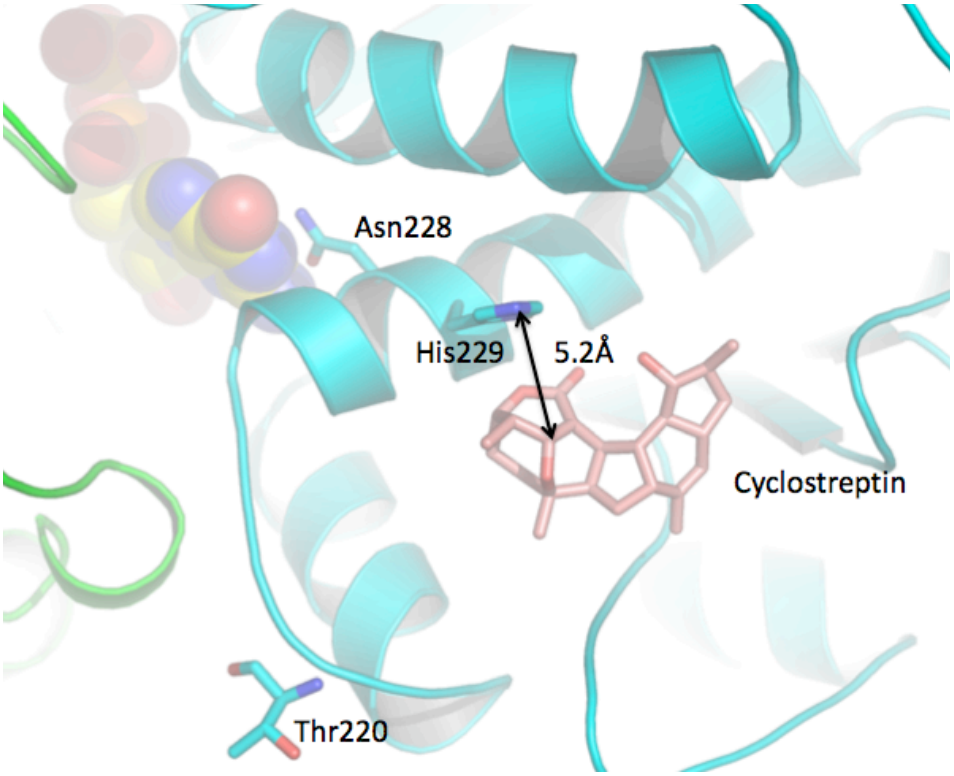

Figure 2-5. One of the docked poses in the PTX binding site using AutoDock4 flexible residue docking is illustrated. The distance between C2 on cyclostreptin and the pyridine-like nitrogen on His229 is 5.2 Å.

In the GDP binding site, the closest distance between the C2 on cyclostreptin and the side chain nitrogen on Asn228 is 4.5 Å. In another pose, the distance between C2 on cyclostreptin and nitrogen on Asn228 is 6.6 Å. We also measured the distance between the side chain oxygen on Asn228 and the C2 on cyclostreptin. In two of these poses, this distance is closer than 5 Å, one of these pose has a distance of 3.2 Å and the other pose has a distance of 3.4 Å. We will discuss the docking result later in the discussion part referring the activity of cyclostreptin.

In the pore area, no pose has a distance between the C2 on cyclostreptin and the side chain oxygen of Thr220 closer than 6Å. We also measured the distance between the C2 on cyclostreptin and the oxygen on Thr221 to be 3.5Å (shown in **Figure 2-6**).

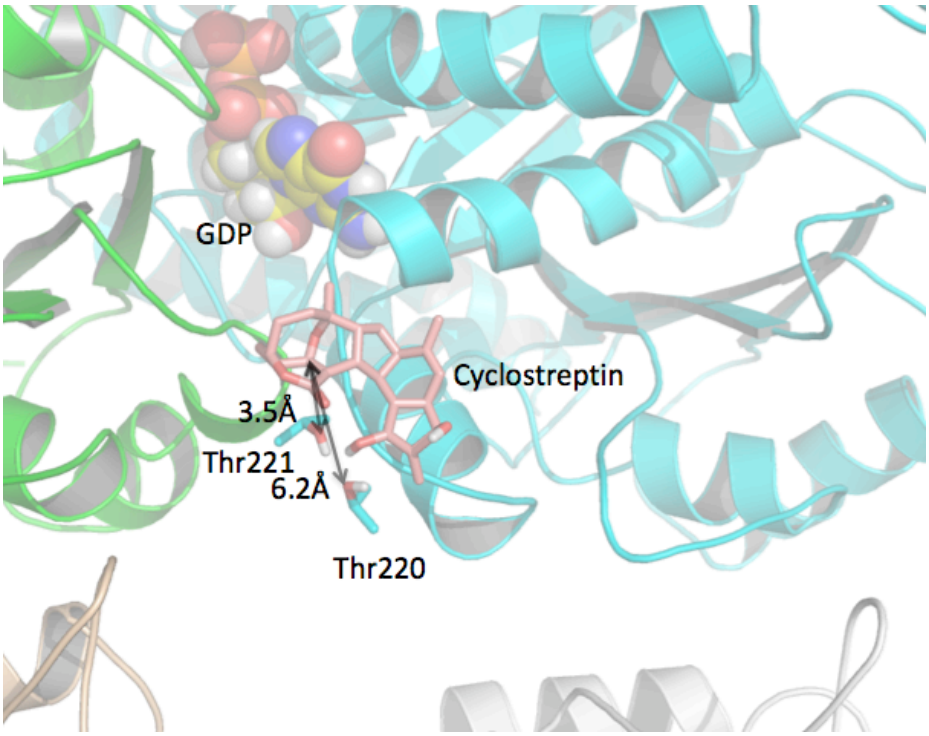

Figure 2-6. One of the docked poses in the pore area using AutoDock4 flexible residue docking is illustrated. The distance between C2 on cyclostreptin and the oxygen on Thr221 is 3.5 Å, and the distance between C2 on cyclostreptin and the oxygen on Thr220 is 6.2 Å.

Induced fit docking

Three independent induced fit dockings (IFD) were performed in the Maestro8.0.308[46] graphical user interface for all of the three sites, the PTX binding site, the GDP binding site and the pore area. In the first stage of the IFD protocol, Glide was used to generate 20 initial poses; the SP scoring function was used in all docking stages. Further in the second stage, a protein refinement was performed around 5 Å of the initial poses. After successful active-site modification, a glide re-dock was performed to generate a final 20 docking poses.

In the PTX binding site, we measured the following three distances.

(1). The distance between C2 on cyclostreptin and the side chain oxygen on Asp226 is large in all of these returned poses. The nearest distance between them is larger than 6 Å.

(2). The nearest distance between the C2 on cyclostreptin and the nitrogen on His229 in all of these returned poses is 4.0 Å. The corresponding pose is shown in **Figure 2-7**.

(3). Arg278 also locates very near cyclostreptin in most of these returned poses, which offers an H-bond for cyclostreptin to dock into the PTX pocket. One of these poses is shown in **Figure 2-8**. In this figure, there are two main hydrogen bonds, one is between cyclostreptin and Arg278 side chain, and the other is between cyclostreptin and the Asp226 side chain.

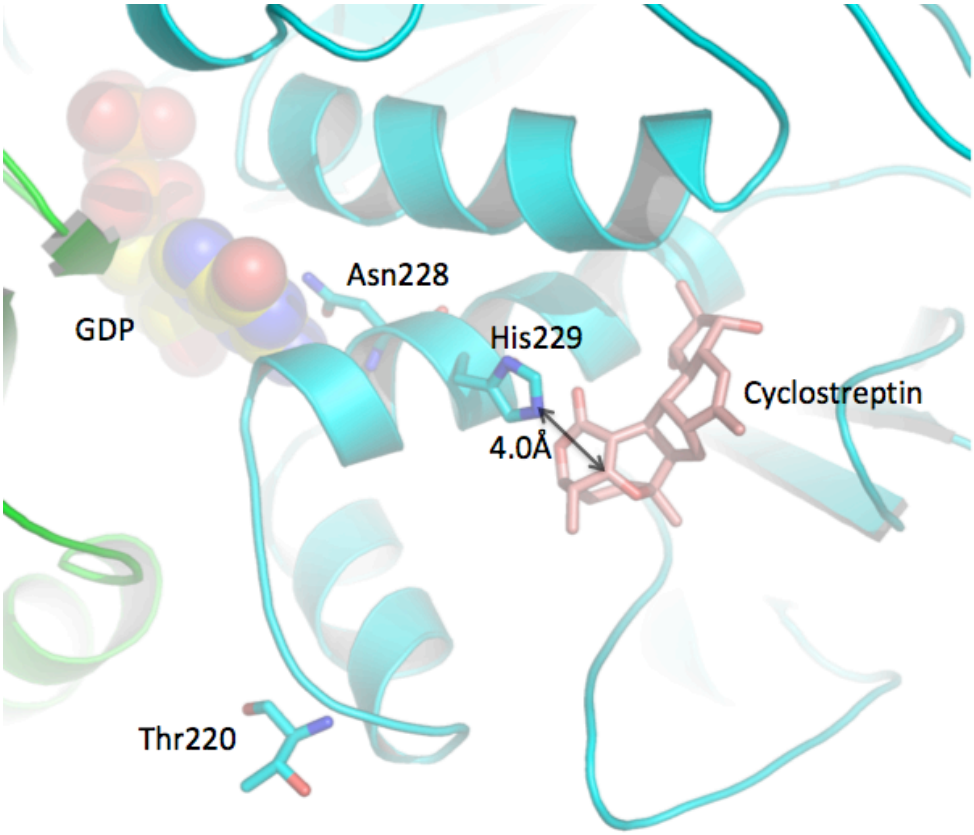

Figure 2-7. One of the docked poses in the PTX binding site using Induced Fit Docking is illustrated. The distance between the C2 on cyclostreptin and the pyridine-like nitrogen on His229 is 4.0 Å.

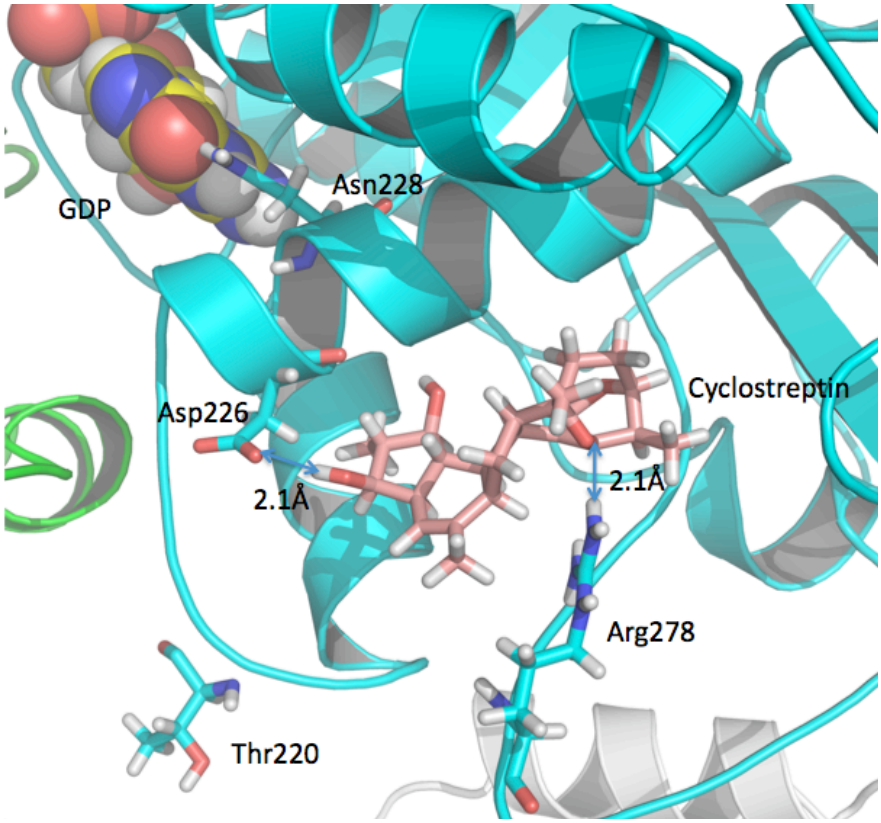

Figure 2-8. One of the docked poses in the PTX binding site using Induced Fit Docking is illustrated. This pose shows several hydrogen bonds between cyclostreptin and other residues.

In the GDP binding site, we measured the distance between the C2 on cyclostreptin and the side chain nitrogen on Asn228. The nearest distance is predicted to be 6.2 Å, as shown in **Figure 2-9**. Among the returned poses, there are other poses that have a shorter distance between the C2 on cyclostreptin and other residues. For example, as shown in **Figure 2-10,** the distance between the C2 on cyclostreptin and the side chain oxygen on Thr223 is 3.4 Å and the distance between the C2 on cyclostreptin and the side chain oxygen on Asp226 is 3.7 Å.

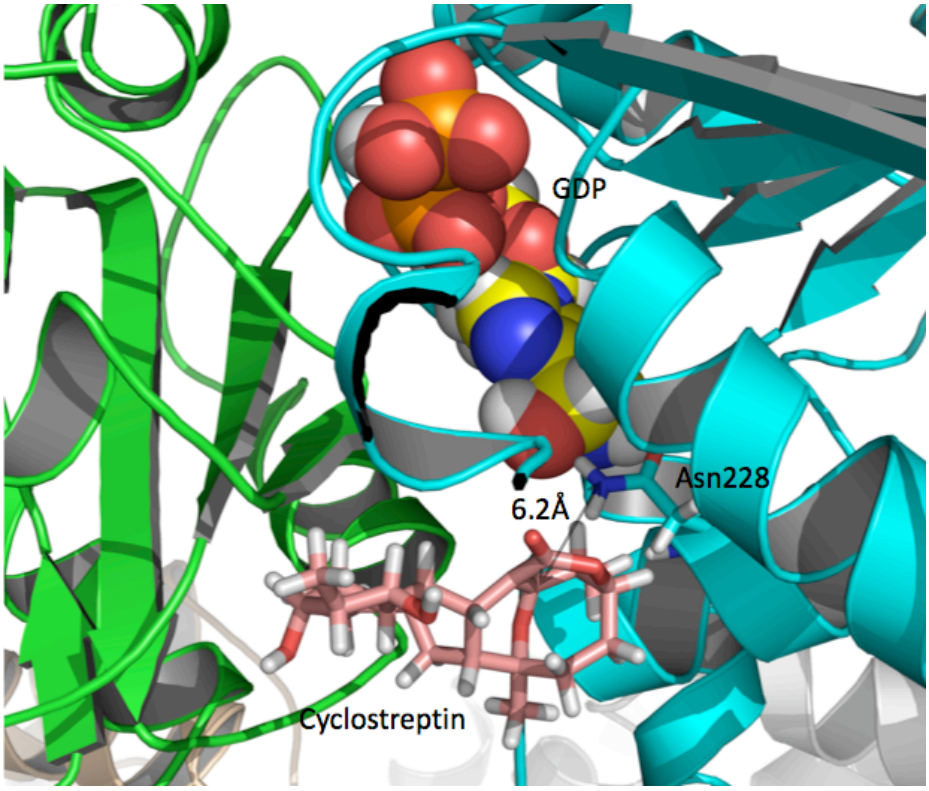

Figure 2-9. One of the docked poses in the GDP binding site using Induced Fit Docking is illustrated. The distance between the C2 on cyclostreptin and the nitrogen on Asn228 is 6.2 Å, which is the nearest distance between these two atoms.

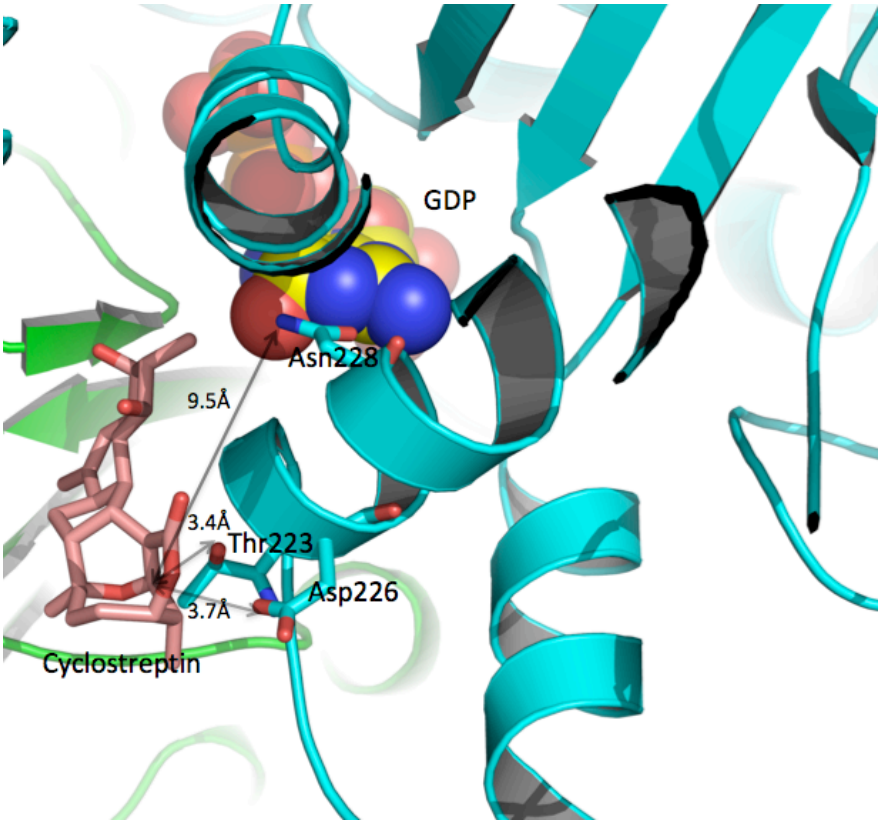

Figure 2-10. One of the docked poses in the GDP binding site using Induced Fit Docking is illustrated. The distance between the C2 on cyclostreptin and the oxygen on Thr223 is 3.4 Å and the distance between the C2 on cyclostreptin and the oxygen on Asp226 is 3.7 Å.

In the pore area, the distance between the C2 on cyclostreptin and the side chain oxygen on Thr220 was measured. The nearest distance among all of these returned poses is predicted to be 7.0 Å.

Since we thought that the cyclostreptin's cytotoxicity might come from its displacement of GDP[47], it is interesting to compare the binding behavior of cyclostreptin and GDP in the GDP binding site. Another induced fit docking of cyclostreptin was performed in the GDP binding site in which GDP was removed. The protocol of the

calculation is identical to the one in the GDP binding site we performed previously. The results show that cyclostreptin is able to dock into the GDP binding site, however the distance between the side chain nitrogen on Asn228 and the C2 on cyclostreptin is large.

Discussion:

Based on the new model and the new two-step mechanism for MSAs binding to microtubules discussed in the Introduction, we would like to test if cyclostreptin is able to dock into the microtubule pore area and the PTX binding site, and how it could dock into these pockets. This is of significance for understanding the binding characteristics of cyclostreptin at a molecular level. Our goal is to determine if there are realistic and preferred poses in the binding sites for cyclostreptin to form chemical bonds with nucleophilic residues on the microtubule near the pore area and in the PTX binding site.

AutoDock blind docking to the microtubule pore

AutoDock Blind Docking was performed to explore where the cyclostreptin molecule can be docked into the microtubule pore. From Figure 2-3, we can clearly see that cyclostreptin can dock into all three main areas in microtubules, which are the PTX binding site, the GDP binding site and the pore area. The two binding sites reported by Buey[42] were found in the blind docking, but there is one more binding site, which is the GDP binding site. This binding site is also in the interior of the microtubule, like the PTX binding site. There are several reasons for considering this as a binding site. First we can consider the GDP binding site as a high affinity site. When PTX or another molecule occupies the PTX binding site, the GDP binding site is conceivably a substitution for

cyclostreptin to bind. When the GDP is removed from the GDP binding site, this pocket is big enough to fit a molecule of a similar size as PTX.

There are also other blind docking poses, which put cyclostreptin in places other than the three binding areas. However, some of these poses are at the edge of the microtubules, where the loops and side chain of the protein are not well defined. Other poses are at the exterior of the microtubule, which is not consistent with the new two-step mechanism of MSAs binding to microtubules. And also these poses only appear once at one place. Thus it is reasonable for us to neglect all these poses, and consider only the poses that sit in the three binding areas we mentioned before.

Glide flexible figand docking

Glide flexible ligand docking fixes the protein in its original coordinates, and searches different space and different torsions for the ligand. It is a relatively cheap calculation for placing the ligand into a docking pocket. A set of glide flexible ligand dockings was performed to generate some general information on whether cyclostreptin can be docked into the three binding pocket we discovered from the AutoDock blind docking.

A detailed analysis of the returned poses was performed by looking into the interaction between cyclostreptin and different nucleophiles near the three docking areas, especially interaction between the nucleophiles on Thr220, Asp226, Asn228, His229 and the cyclostreptin molecule (from our interpretation of the MS data). From the results, we found that cyclostreptin can be docked into the paclitaxel binding site. However, none of the returned poses suggest that there is any possibility for nucleophilic atoms on Asp226,

Asn228 or His229 to attack the C2 atom on cyclostreptin and form a covalent bond with the C2 atom. This conclusion is derived from measuring the distances between the C2 atom on cyclostreptin and the active atoms on these nucleophiles. The docking results also reveal that cyclostreptin is able to dock into the pore area, yet the results suggest it is not possible for Thr220 to interact with cyclostreptin. Finally, by docking cyclostreptin to the GDP binding site with GDP in the microtubule pore, we found that even if we scaled down the van der Waals radii from 0.80 Å to 0.25 Å, cyclostreptin still cannot dock into the GDP binding site. This discovery does not astonish us, because GDP is already sitting in the GDP binding site, if the protein is fixed, there's no other room to accommodate the cyclostreptin in the GDP pocket. Thus we cannot see any of the cyclostreptin poses in the GDP binding site by Glide flexible ligand docking. We hope that by allowing the protein to move around the docking pocket, cyclostreptin will be able to dock into the GDP binding site.

AutoDock flexible residue docking

AutoDock flexible residue docking was then used to explore how the cyclostreptin molecule will dock into the three areas identified from AutoDock blind docking with several selected residues to be flexible. AutoDock flexible residue docking is a relative cheap flexible protein calculation compared to other programs, since it is only allows the selected residues to search different side chain torsions, no backbone movement is allowed in AutoDock's flexible residue docking. However, by moving the protein residues, more cyclostreptin binding poses will be generated compared to the rigid protein-docking algorithm.

We Performed AutoDock flexible residue docking in the following three areas we identified from AutoDock blind docking. When we performed these dockings, we allow GDP in its original binding site to mimic the wide type protein.

Figure 2-11 superimposes all of the top 20 binding poses in the PTX binding site. All of these poses clustered together, demonstrating that there is a well-defined docking pocket for cyclostreptin to dock into. The side chain of selected protein residues are subject to move to accommodate the cyclostreptin molecule, however, in the top 20 poses, the protein residues do not move a lot, since the cyclostreptin molecule has enough space to reside in the PTX pocket.

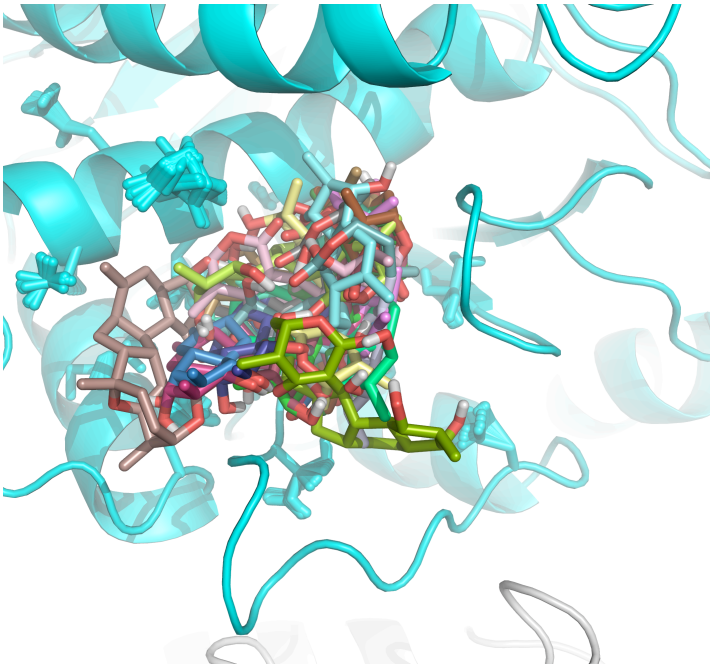

Figure 2-11. Superposition of the top 20 docking poses in the PTX binding site from AutoDock flexible residue docking

In the PTX binding site, we first measured the distance between the side chain nitrogen on Asn228 and the C2 carbon on cyclostreptin. Since Asn228 was reported by

Buey[42] and coworkers in the high affinity binding site and can potentially serve as a nucleophile, which in the interior of the microtubule and can attack and then form a covalent bond with cyclostreptin. Unfortunately, none of the returned poses predicted that cyclostreptin reacts with Asn228, since the distances between the side chain nitrogen on Asn228 and the C2 carbon on cyclostreptin in all of these poses are too large to have any interaction.

Experimental data by Vanderwal and co-workers showed[43] that imidazole is suggested to be an effective nucleophile to attack cyclostreptin. And since His229 is one residue after the Asn228, it is possible for the cyclostreptin labeling transfer from one residue to a nearby residue in the mass spectrum experiment compatible with movement of the label from His229 to Asn228, the site reported by Buey[42]. Thus I measured the distance between the C2 on cyclostreptin and the pyridine-like nitrogen on His229 to see if there are some possibilities for His229 to interact with cyclostreptin. The docking results do not give us any positive docking poses regarding His229. In all of these poses, the nearest distance between the pyridine-like nitrogen on His229 and the C2 on cyclostreptin is 5.2 Å, which is too far for the His229 nucleophile to attack cyclostreptin, although the pyridine-like nitrogen on His229 has a perfect orientation to attack the C2 carbon on cyclostreptin, as shown in **Figure 2-5**.

In our experiment, we discover that residue Asp226 in the PTX binding site is found really close to the C2 carbon on cyclostreptin several times. One of these poses that interest us is illustrated in **Figure 2-4**. As shown in the figure, the distance between the side chain oxygen on Asp226 and the C2 on cyclostreptin is predicted to be 3.6Å. Furthermore, Asp226 resides in a right position to attack cyclostreptin, both of which are

required for a conjugate addition. These poses indicate the possibility that the side chain oxygen on Asp226 is able to engage in a nuclophilic attack at the C2 carbon of cyclostreptin and form a covalent bond between them. Since Asp226 is found several times near cyclostreptin, it is worth to consider whether Asp226 can really be a residue to form covalent bond with cyclostreptin. Although Asp226 was not the residue reported by Buey and coworkers[42] to form a chemical bond with cyclostreptin in their mass spectrum data, my first thought was that since Asp226 is only 2 amino acids before Asn228, and both of Asp226 and Asn228 are in the same helix near the paclitaxel binding site, it might be possible for the mass spectrum label to transfer from Asp226 to Asn228. However, by closely analyzing Buey's mass spectrum, we noticed that they chopped the residues exactly before Asn228, and found cyclostreptin signals in the piece after Asn228. For this reason, although Asp226 is a perfect nucleophile to interact with cyclostreptin in both nucleophilic experiment and the AutoDock flexible residue docking experiment, it was not found in the mass spectrum experiment.

From the nucleophilic experiment, we note that cysteine may also serve as a perfect nucleophile to attack cyclostreptin[43]. We measured the distance between the side chain sulfur atom on Cys213 and the C2 carbon on cyclostreptin to see if there are some possibilities for Cys213 to nucleophilic attack cyclostreptin. In the same pose we discovered a short distance between Asp226 and cyclostreptin (**Figure 2-4**), Cys213 is also located nearby, the distance between the sulfur atom on Cys213 and the C2 carbon on cyclostreptin in this pose is 5.1Å, making Cys213 also possible to attack Cyclostreptin. Unfortunately, there's no mass spectrum evidence support Cys213 to be a residue for cyclostreptin to react with[42].

Figure 2-12 captures the top 20 ranking poses in the GDP binding site from AutoDock flexible residue docking. As we can see from this picture, cyclostreptin is not actually docked into the GDP binding site, since GDP already occupies this pocket. However, cyclostreptin is able to find an area near the GDP binding site to dock into. In this case, flexible residue is necessary to accommodate cyclostreptin in this area. At the same time, cyclostreptin is not so clustered in the top 20 poses compared to the docking result from the PTX binding site, since it searches the area nearby for any possible docking poses.

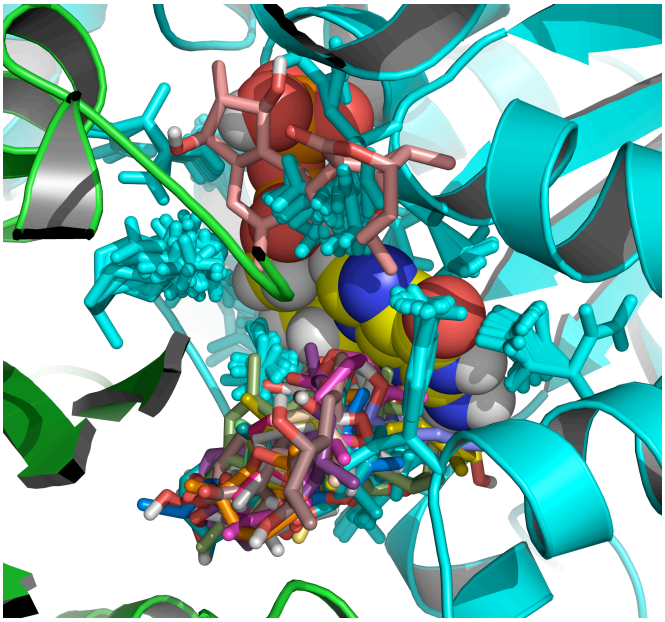

Figure 2-12. Superposition of the top 20 docking poses in the GDP binding site from AutoDock flexible residue docking

In the GDP binding site, we also explored possible residues that can react with cyclostreptin around the binding site. By measuring the distance between the side chain nitrogen atom on Asn228 and the C2 atom on cyclostreptin, we found that the nearest distance between these two atoms is 4.5Å, however, the orientation of the Asn228 residue

makes it impossible to attack and form chemical bond with cyclostreptin. In another pose, the distance between the side chain nitrogen atom on Asn228 and the C2 atom on cyclostreptin is 6.6Å. In this pose, Asn228 has a better orientation to react with cyclostreptin; however, this distance is too far for Asn228 to interact with cyclostreptin.

Figure 2-13 is a superimposition of the top 20 poses in the pore area from AutoDock flexible residue docking. This figure illustrates that there is no well-defined docking pocket for cyclostreptin to reside in; the top 20 poses are scattered around in the pore area.

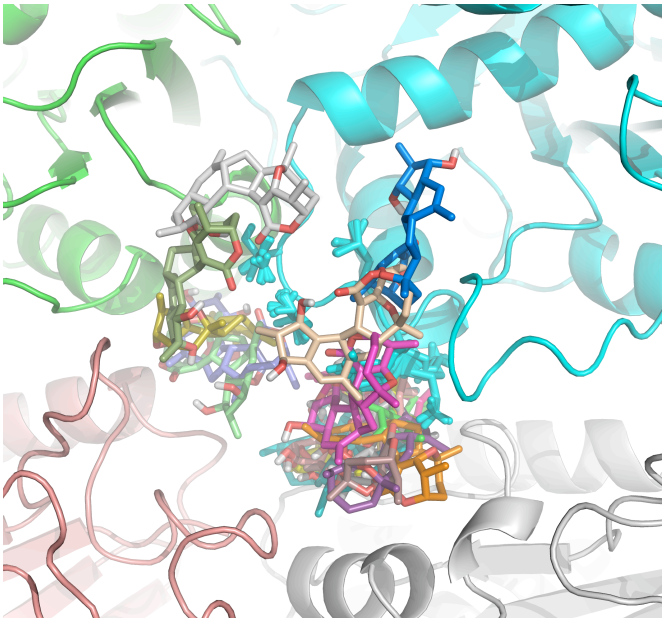

Figure 2-13 Superposition of the top 20 docking poses in the pore area from AutoDock flexible residue docking

Although there is no well-defined docking pocket for cyclostreptin to dock into the pore area, we still need to explore whether some of the residues have the possibility to necleophilically attack cyclostreptin. We measured the distance between the side chain

oxygen atom on Thr220 and the C2 atom on cyclostreptin to see if Thr220 can attack cyclostreptin in agreement with the mass spectrum data[42]. Unfortunately, in our docking experiment, there is no pose with the distance between the side chain oxygen atom on Thr220 and the C2 atom on cyclostreptin nearer than 6Å. However, one of these poses reviews that there are some possibility for cyclostreptin to interact with Thr221, since the distance between the side chain oxygen atom on Thr221 and the C2 atom on cyclostreptin is 3.5Å (**Figure 2-6**). Thr221, though not indicated in the mass spectrum data, is one residue behind Thr220. According to what was discussed about a residue label transferring during the mass spectrum experiment, Thr221 is a possible candidate in the low affinity binding site on the exterior of the microtubule.

Induced fit docking

Induced fit docking is a flexible ligand and protein docking algorithm, which sequentially uses the Glide[1,29] docking algorithm, Prime protein refinement[31] and Glide redocking algorithm. Using this combination, both the ligand and the protein are allowed to be flexible. Compared to AutoDock flexible residue docking, induced fit docking is able to move the protein backbone together with the side chains, and is especially accurate in predicting protein loop movement. A set of induced fit dockings was performed to the three areas discovered in the blind docking, the PTX binding site, the GDP binding site, and the pore area. The results were compared with those from AutoDock4.

Figure 2-14 superimposes the top 20 docking poses in the PTX binding site from induced fit docking. This picture again shows that there is a well-defined docking pocket in the PTX binding site as shown in **Figure 2-11**. The backbone of the protein does not

need to change much in the top 20 poses to accommodate cyclostreptin in the docking pocket, which is consistent with the results come from AutoDock flexible residue docking.

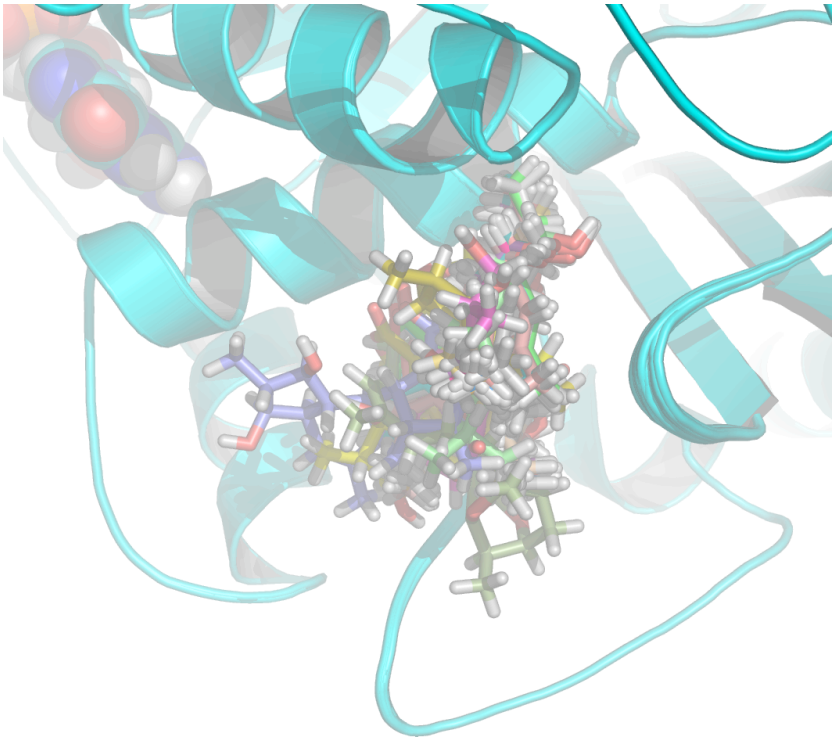

Figure 2-14. Superposition of the top 20 docking poses in the PTX binding site from induced fit docking

In the PTX binding site, we are interested to see if there are some possibilities for Asn226 or other residues to react with cyclostreptin. In most of these returned poses, Asp226 experiences very nice orientations to interact with cyclostreptin, however the distance between the side chain oxygen atom on Asp226 and the C2 atom on cyclostreptin is far (almost 10Å). Among all of these returned poses, one indicates that there is another residue that has the ability to form chemical bond with cyclostreptin, His229. As shown in **Figure 2-7**, the distance between the nitrogen atom on His229 and

the C2 atom on cyclostreptin and is about 4Å, and the orientation of His229 also makes it possible to engage in nucleophilic attack on cyclostreptin. Arg278 plays another important role in some of these docking poses. It locates near cyclostreptin in most of these poses, offering an H-bond for cyclostreptin to dock into the PTX pocket. As **Figure 2-8** shows, there are two important hydrogen bonds between cyclostreptin and the protein, which are the Asp226-cyclostreptin and the Arg278-cyclostreptin hydrogen bonds.

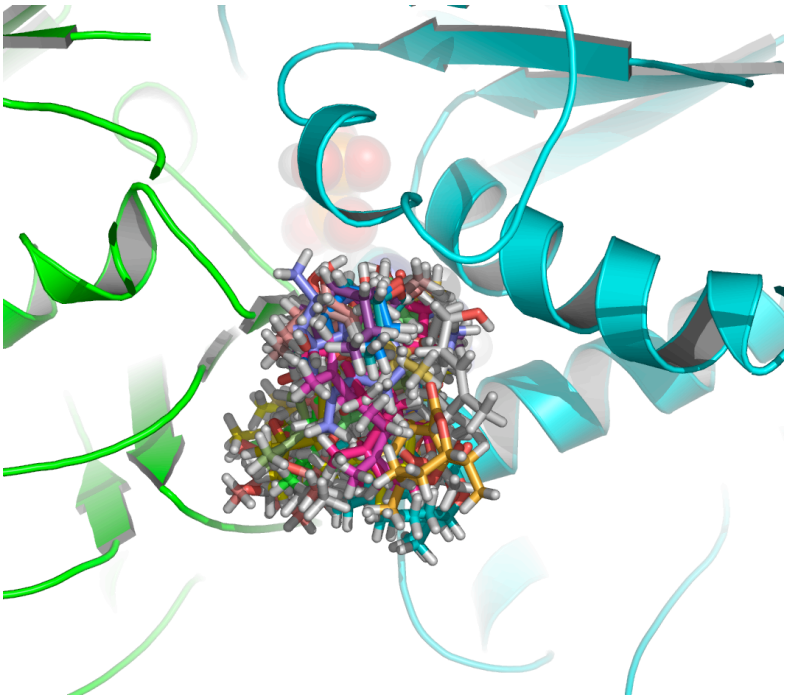

Figure 2-15. Superposition of the top 20 docking poses in the GDP binding site from induced fit docking

Figure 2-15 shows how the top 20 docking poses differ from each other from induced fit docking. As we saw in the AutoDock results, cyclostreptin is not really docked into the GDP binding site, since GDP is already sitting there. However, cyclostreptin did find

a way to put itself into the protein structure. The docking area in which cyclostreptin resides is near the pore area. Thus the docking area is not so well defined compared to the PTX binding site.

In the GDP binding site, the shortest distance between the side chain nitrogen on Asn228 and the C2 on cyclostreptin is predicted to be 6.2Å, as shown in **Figure 2-9**. The orientation of Asn228 seems to be suitable for nucleophile attack on cyclostreptin. However, the distance between them is too far for any reaction to take place. Among the returned poses, some other residues reside nearby and have the possibility to attack cyclostreptin. For example, as shown in **Figure 2-10,** the distance between the side chain oxygen atom on Thr223 and the C2 atom on cyclostreptin is 3.4Å, and the distance between the side chain oxygen atom on Asp226 and the C2 atom on cyclostreptin is 3.7Å. In this pose, the orientations of both Thr223 and Asp226 are excellent to undergo a conjugate addition. It is extremely interesting to find that in the GDP binding site, there are some possibilities for Asp226 to interact with cyclostreptin, since in the original microtubule pore structure and the AutoDock flexible residue docked structure, the Asp226 residue is pointing toward the PTX binding pocket. However, in this particular induced fit docking pose, the Asp226 is pointing toward the GDP binding pocket. Why is it that in this induced fit docking result, we cannot see a similar orientation of Asp226 as observed by the AutoDock flexible residue docking result? One possible explanation is that Prime protein refinement not only moves the protein side chains, it also moves the protein backbones, making the Asp226 residue able to point to the GDP binding pocket.

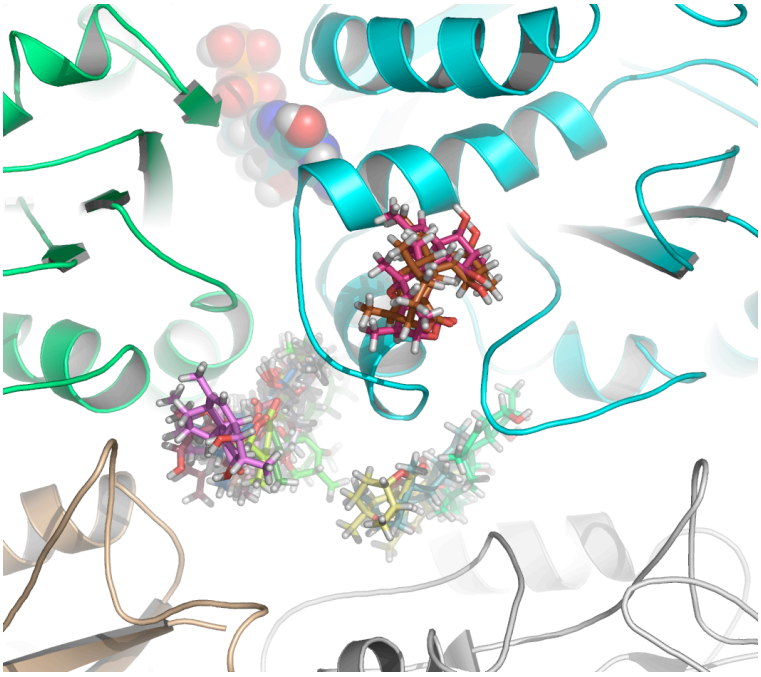

Figure 2-16. Superposition of the top 20 docking poses in the pore area from induced fit docking

By superimposing the top 20 docking poses in the pore area from induced fit docking (**Figure 2-16**), we are not surprised to find that there's not a well defined docking pocket for cyclostreptin as we found in AutoDock flexible residue docking result. There are three main docking areas for cyclostreptin to reside in the pore area, one of them is near the exterior of the microtubule, one of them is near the Thr220 residue, and the one is almost inside the PTX binding site, since we made the grid box big enough to cover the PTX binding site.

In the pore area, the shortest distance between the side chain oxygen atom on Thr220 and the C2 atom on cyclostrptin is 7.0 Å; too far for Thr220 to interact with cyclostreptin.

As illustrated above, cyclostreptin sits between two tubulin dimers in the pore area. Only the αβ-dimer crystal structure can be found in the Protein Data Bank (PDB)[48] with 3.5Å resolution. The two-dimer protein we used in our calculations was derived from docking the tubulin into a microtubule model, with a resolution of 8Å[41]. Although our model is good in the PTX and GDP binding site, there might be some differences between the model and the real microtubules in the pore area, making it difficult to predict the docking poses of cyclostreptin and the interactions between cyclostreptin and the protein.

Summary and Conclusions:

The result of the blind docking using AutoDock4 convinces us that there are three main areas for cyclostreptin to dock into microtubules. These include the famous PTX binding site, the GDP binding site, and the area near the pore of two dimers.

The Glide docking suggests that cyclostreptin is able to dock into the PTX binding site, the pore area, but unable to dock into the GDP binding site. Also the results reveal that there is little possibility for the nucleophiles Thr220, Asn228 or Asp226 to attack cyclostreptin under docking conditions in which the protein residues are held rigid.

Results from flexible residue docking using AutoDock4 and induced fit docking using Maestro8.0.308 both reveal that cyclostreptin is able to dock into the three areas found in previous blind docking. These are the same three sites explored by Glide flexible ligand docking: the PTX binding site, the GDP binding site and the pore area. Calculations with both of the docking programs suggest that there is little possibility for

Thr220 and Asn228 to interact with cyclostreptin. However, there are some possibilities for Cys213, Thr221, Thr223, Asp226 or His229 to do so.

The MS data[42] showed that there are two residues, Thr220 and Asn228, which are able to form covalent bond with cyclostreptin. However, since His229 is only one residue after Asn228, there might be some possibilities for His229 to form a covalent bond with cyclostreptin in microtubules first. Then the amino acid fragment with cyclostreptin covalently bond to His229 might undergo rearrangement in the MS before it has been recorded. Thus, there might be the possibility that cyclostreptin actually bonds to His229 instead of Asn228.

Vanderwal[43] tested the reactivity of cyclostreptin with several nucleophiles. However, they did not do test on alcohol groups. As we can see from their paper, they synthesized the cyclostreptin molecule in ethanol. This indicates that Thr220 may not serve as a nucleophile since cyclostreptin is stable in ethanol. Thus, it seems that Thr220 is not a preferred nucleophile if there are other more nucleophilic amino acids with proper orientations around cyclostreptin. Also, there is no study of the reactivity between alcohol and cyclostreptin. However, cyclostreptin can be synthesized in methanol[43]. In this sense, whether Asn228 can be a nucleophile to attack cyclostreptin is still a mystery.

Part 3. Possible Interactions between Ligand Trifluoromethyl Groups and Proteins

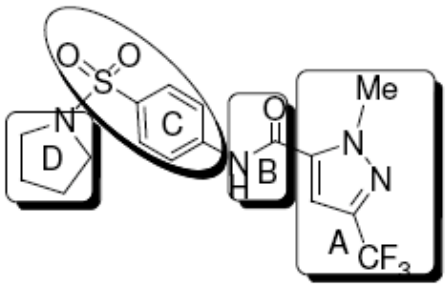

Figure 3-1. The structure of compound 16677

Introduction

Measles virus is one of the most infectious pathogens we have ever known[49]. Though we have ribavirin[50,51] to treat measles virus infections, it is the only drug available these days. Also due to the low coverage[52] of this drug and limited efficacy[53], there are still large numbers of people who die from measles virus infections every year. The development of new anti-measles compounds is really important in controlling this disease.

Compound 1-methyl-3-(trifluoromethyl)-*N*-[4-(pyrrolidinylsulfonyl)phenyl]-1H-pyrazole-5-carboxamide, 16677 (shown in **Figure 3-1**) was found to be the most potent cell-based high-throughput screening (HTS) inhibitor against MV identified from a 30,000 compound library[54,55,56]. We also found in the experiment that substitution of the trifluoromethyl group in compound 16677 with a methyl or a *t*-butyl group completely abrogates the inhibitory activity of this compound[56].

Methods and Results

In order to gain insight into the possible role of the pyrazole CF_3 as an enhancer of MV inhibition and to investigate more generally the structural influence of CF_3 groups in protein-bound ligands, Relibase+[57] was used to search for such protein-ligand complexes in the Protein Data Bank (PDB)[48]. A total of 132 ligands containing the CF_3 moiety was returned from the search.

ReliView was used to analyze the interaction between CF_3 groups and proteins in cluster of protein side-chains, water, ions, or other small molecules within 4Å. In the returned hits, less than a dozen trifluoromethyl groups were located in hydrophobic environments, while 15 were directed into the aqueous layer surrounding the proteins. Carbon-fluorine bonds in 117 complexes were able to participate in at least one CF---HX (X = O, N or S) interaction in which F---X distances ranged from 2.7- 3.6 Å.

Discussion

It has been argued that fluorine rarely engages in hydrogen bonds in small molecule X-ray crystal structures[58]. However, in protein pockets where ligands are constrained by a variety of forces, it appears to be more possible for fluorine to experience H-bonding interactions with its surroundings.

F---X distances beyond 3.0 Å can be regarded as dipole-dipole interactions that most likely provide small stabilizing contributions (< 1 kcal/mol) for the observed binding poses. An example is presented in **Figure3-2** (PDB code 1NCR[59]), in which one of the CF_3 fluorine atoms has a short contact with the backbone NH of Tyr144.

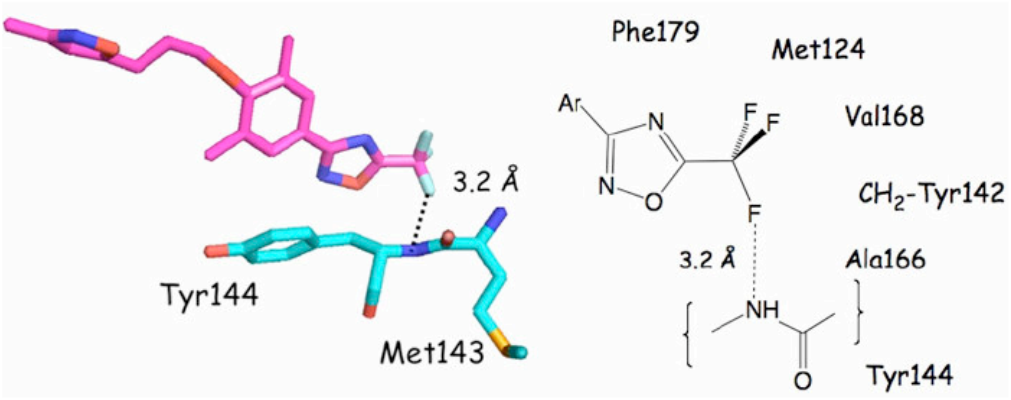

Figure 3-2. One of the CF_3 fluorine atoms interacts with the backbone NH of Tyr144 in 1NCR.

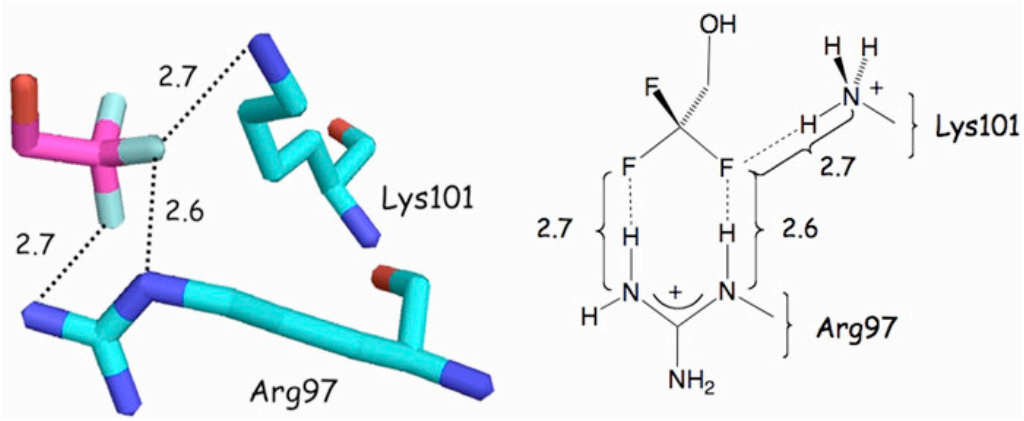

Figure 3-3. In 1P2S, the CF_3 group is situated between Arg97 and Lys101 side chains by bidentate and monodentate hydrogen bonds, respectively.

A subset of 28 cases involved Arg, Lys and His residues that direct N-H bonds toward fluorine. One interesting pose (1P2S[60]) located the fluorine between Arg and Lys side chains as shown in **Figure 3-3**. The topographical representations shows that Arg97 forms a bidentate contact with two fluorine atoms, while Lys101 interacts with one

fluorine in the same pair; all of which involve F---H distances of 2.6-2.7 Å. The latter are 0.3-0.4 Å smaller than the sum of the van der Waals radii[33] (N 1.55, F 1.47 Å).

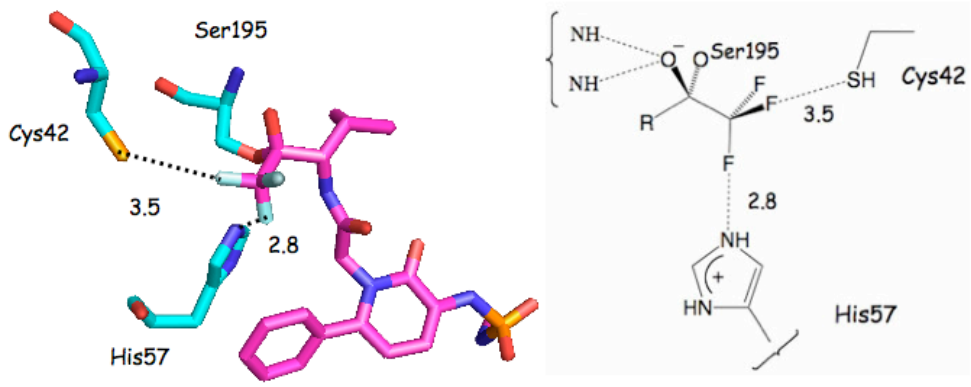

Figure 3-4. F—HS hydrogen bond and a charge dipole interaction between a ligand C-F bond and His57 are illustrated in 1EAS.

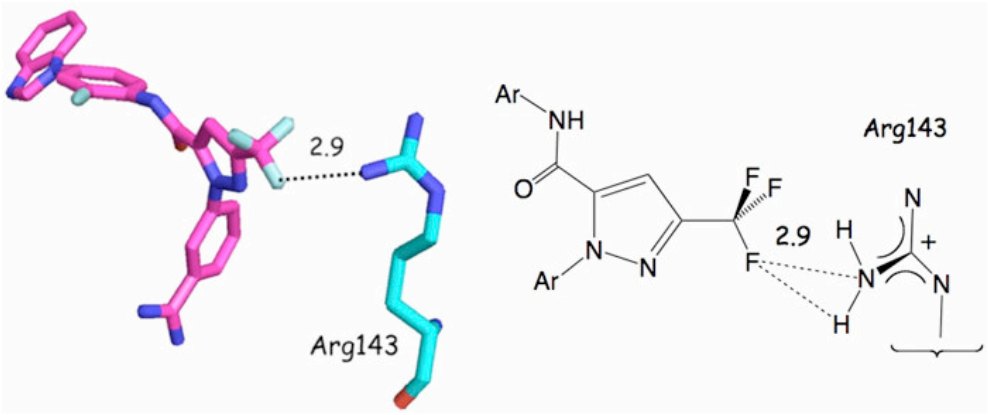

Figure 3-5: The CF_3 group of the pyrazole ligand interacts with the cationic Arg143 side chain in 1X7A.

Figure 3-4 shows that a trifluoromethyl ketone(1EAS[61]) has a weak interaction with the SH of Cys42 and a stronger interaction with His57.

Four protein ligands are found similar to that of compound 16677, which has a CF_3 group in the pyrazole ring. Three of these (1X7A[62], 1CX2[63] and 6COX[63]) have interactions between the CF_3 fluorines and a single Arg residue (as **Figure3-5** shown). In the fourth protein (1OQ5[64]), the trifluoromethyl group is in a hydrophobic region on the surface of the protein.

If the binding site for the trifluoromethyl group in the MV RNA-dependent RNA polymerase is hydrophobic or exposed to solvent, then the substitution of CF_3 in 16677 with CH_3 is unlikely to cause complete loss of activity as observed.

Summary and Conclusions

Thus, we conclude that the pyrazole-CF_3 in the highly active MV inhibitor examined in this work is likely to be docked into a pocket that is surrounded by Arg, Lys and/or His. This prediction is important in developing new potent anti-measles candidates with similar or more bioactivity and improved solubility.

References:

1 Friesner, R. A. et al., Glide: a new approach for rapid, accurate docking and scoring. 1. Method and assessment of docking accuracy. *Journal of medicinal chemistry* **47** (7), 1739 (2004).

2 Jordan, Mary Ann and Wilson, Leslie, Microtubules as a target for anticancer drugs. *Nat. Rev. Cancer* **4** (4), 253 (2004).

3 Ernest, Hamel, Antimitotic natural products and their interactions with tubulin. *Medicinal Research Reviews* **16** (2), 207 (1996).

4 Wani, Mansukhlal C. et al., Plant antitumor agents. VI. Isolation and structure of taxol, a novel antileukemic and antitumor agent from Taxus brevifolia. *J. Amer. Chem. Soc.* **93** (9), 2325 (1971).

5 Schiff, Peter B., Fant, Jane, and Horwitz, Susan B., Promotion of microtubule assembly in vitro by taxol. *Nature (London)* **277** (5698), 665 (1979).

6 Goodman, J.; Walsh, V. The Story of Taxol: Nature and Politics in the Pursuit of an Anti-Cancer Drug. Cambridge University Press. 2001, ISBN 0 521 56123 X

7 http://www.accessdata.fda.gov/scripts/cder/onctools/summary.cfm?ID=123

8 Mastropaolo, D. et al., Crystal and molecular structure of paclitaxel (taxol). *Proceedings of the National Academy of Sciences of the United States of America* **92** (15), 6920 (1995).

9 Kingston, D. G., Bane, S., and Snyder, J. P., The taxol pharmacophore and the T-taxol bridging principle. *Cell Cycle* **4** (2), 279 (2005); Geney, RaphaÎl et al., Use of the Tubulin Bound Paclitaxel Conformation for Structure-Based Rational Drug Design. *Chemistry & Biology* **12** (3), 339 (2005).

10 Nogales, E., Wolf, S. G., and Downing, K. H., Structure of the alpha beta tubulin dimer by electron crystallography. *Nature* **391** (6663), 199 (1998).

11 Lowe, J., Li, H., Downing, K. H., and Nogales, E., Refined structure of alpha beta-tubulin at 3.5 A resolution. *J Mol Biol* **313** (5), 1045 (2001).

12 Snyder, J. P. et al., The binding conformation of Taxol in beta-tubulin: a model based on electron crystallographic density. *Proc Natl Acad Sci U S A* **98** (9), 5312 (2001).

13 Ganesh, T. et al., The bioactive Taxol conformation on beta-tubulin: experimental evidence from highly active constrained analogs. *Proc Natl Acad Sci U S A* **101** (27), 10006 (2004).

14 Paik, Y. et al., Rotational-echo double-resonance NMR distance measurements for the tubulin-bound Paclitaxel conformation. *J Am Chem Soc* **129** (2), 361 (2007).

15 Geney, R. et al., Use of the tubulin bound paclitaxel conformation for structure-based rational drug design. *Chem Biol* **12** (3), 339 (2005).

16 Li, Y. et al., Conformation of microtubule-bound paclitaxel determined by fluorescence spectroscopy and REDOR NMR. *Biochemistry* **39** (2), 281 (2000).

17 Alcaraz, A. A., Mehta, A. K., Johnson, S. A., and Snyder, J. P., The T-Taxol conformation. *J Med Chem* **49** (8), 2478 (2006).

18 Johnson, S. A., Alcaraz, A. A., and Snyder, J. P., T-Taxol and the electron crystallographic density in beta-tubulin. *Org Lett* **7** (25), 5549 (2005).

19 https://www.schrodinger.com/ProductDescription.php?mID=6&sID=15&cID=0

20 https://www.schrodinger.com/ProductDescription.php?mID=6&sID=15&cID=0

21 Fariborz Mohamadi, Nigel G. J. Richards Wayne C. Guida Rob Liskamp Mark Lipton Craig Caufield George Chang Thomas Hendrickson W. Clark Still, Macromodel†-†an integrated software system for modeling organic and bioorganic molecules using molecular mechanics. *Journal of Computational Chemistry* **11** (4), 440 (1990).

22 Rush, T. S., 3rd, Grant, J. A., Mosyak, L., and Nicholls, A., A shape-based 3-D scaffold hopping method and its application to a bacterial protein-protein interaction. *J Med Chem* **48** (5), 1489 (2005).

23 Hawkins, P. C., Skillman, A. G., and Nicholls, A., Comparison of shape-matching and docking as virtual screening tools. *J Med Chem* **50** (1), 74 (2007).

24 Gaussian 03, Revision C.02, M. J. Frisch, G. W. Trucks, H. B. Schlegel, G. E. Scuseria, M. A. Robb, J. R. Cheeseman, J. A. Montgomery, Jr., T. Vreven, K. N. Kudin, J. C. Burant, J. M. Millam, S. S. Iyengar, J. Tomasi, V. Barone, B. Mennucci, M. Cossi, G. Scalmani, N. Rega, G. A. Petersson, H. Nakatsuji, M. Hada, M. Ehara, K. Toyota, R. Fukuda, J. Hasegawa, M. Ishida, T. Nakajima, Y. Honda, O. Kitao, H. Nakai, M. Klene, X. Li, J. E. Knox, H. P. Hratchian, J. B. Cross, V. Bakken, C. Adamo, J. Jaramillo, R. Gomperts, R. E. Stratmann, O. Yazyev, A. J. Austin, R. Cammi, C. Pomelli, J. W. Ochterski, P. Y. Ayala, K. Morokuma, G. A. Voth, P. Salvador, J. J. Dannenberg, V. G. Zakrzewski, S. Dapprich, A. D. Daniels, M. C. Strain, O. Farkas, D. K. Malick, A. D. Rabuck, K. Raghavachari, J. B. Foresman, J. V. Ortiz, Q. Cui, A. G. Baboul, S. Clifford, J. Cioslowski, B. B. Stefanov, G. Liu, A. Liashenko, P. Piskorz, I. Komaromi, R. L. Martin, D. J. Fox, T. Keith, M. A. Al-Laham, C. Y. Peng, A. Nanayakkara, M. Challacombe, P. M. W. Gill, B. Johnson, W. Chen, M. W. Wong, C. Gonzalez, and J. A. Pople, Gaussian, Inc., Wallingford CT, 2004.

25 The atomic coordinates of the PTX-NY ligand structure embedded in a partial β-tubulin protein structure were kindly provided by Professor Iwao Ojima (State University of Stony Brook, Stony Brook, NY)

26 Shanker, N. et al., Enhanced microtubule binding and tubulin assembly properties of conformationally constrained paclitaxel derivatives. *Biochemistry* **46** (41), 11514 (2007).

27 Lindahl, E. , Hess, B. , and Spoel, D. , GROMACAS 3.0: a package for molecular simulation and trajectory analysis. *J. Mol. Mod.* **7** (8), 306 (2001).

[28] David Van Der Spoel, Erik Lindahl Berk Hess Gerrit Groenhof Alan E. Mark Herman J. C. Berendsen, GROMACS: Fast, flexible, and free. *Journal of Computational Chemistry* **26** (16), 1701 (2005).

[29] Halgren, T. A. et al., Glide: a new approach for rapid, accurate docking and scoring. 2. Enrichment factors in database screening. *Journal of medicinal chemistry* **47** (7), 1750 (2004).

[30] Mastropaolo, D. et al., Crystal and molecular structure of paclitaxel (taxol). *Proc Natl Acad Sci U S A* **92** (15), 6920 (1995).

[31] Zhu, K., Shirts, M. R., and Friesner, R. A., Improved Methods for Side Chain and Loop Predictions via the Protein Local Optimization Program: Variable Dielectric Model for Implicitly Improving the Treatment of Polarization Effects. *J. Chem. Theory Comput.* **3** (6), 2108 (2007).

[32] Ganesh, T. et al., Evaluation of the tubulin-bound paclitaxel conformation: synthesis, biology, and SAR studies of C-4 to C-3' bridged paclitaxel analogues. *J Med Chem* **50** (4), 713 (2007).

[33] Bondi, A., van der Waals Volumes and Radii. *J. Phys. Chem.* **68** (3), 441 (1964).

[34] Snyder, J. P., Nevins, N., Cicero, D. O., and Jansen, J., The Conformations of Taxol in Chloroform. *J. Am. Chem. Soc.* **122** (4), 724 (2000).

[35] Sun, L. et al., Design, Synthesis, and Biological Evaluation of Novel C14-C3'BzN-Linked Macrocyclic Taxoids. *J Org Chem* (2008).

[36] Bollag, D. M. et al., Epothilones, a new class of microtubule-stabilizing agents with a taxol-like mechanism of action. *Cancer research* **55** (11), 2325 (1995).

[37] Hung, D. T., Chen, J., and Schreiber, S. L., (+)-Discodermolide binds to microtubules in stoichiometric ratio to tubulin dimers, blocks taxol binding and results in mitotic arrest. *Chemistry & biology* **3** (4), 287 (1996).

[38] Sato, Bunji et al., A new antimitotic substance, FR182877. I. Taxonomy, fermentation, isolation, physico-chemical properties and biological activities. *J. Antibiot.* **53** (2), 123 (2000).

[39] Yoshimura, Seiji et al., A new antimitotic substance, FR 182877. III. Structure determination. *J. Antibiot.* **53** (6), 615 (2000); Sato, B. et al., A new antimitotic substance, FR182877. II. The mechanism of action. *The Journal of antibiotics* **53** (2), 204 (2000).

[40] Edler, M. C. et al., Cyclostreptin (FR182877), an antitumor tubulin-polymerizing agent deficient in enhancing tubulin assembly despite its high affinity for the taxoid site. *Biochemistry* **44** (34), 11525 (2005).

[41] Li, Huilin et al., Microtubule Structure at 8 A Resolution. *Structure (Cambridge, MA, United States)* **10** (10), 1317 (2002).

[42] Buey Ruben, M. et al., Cyclostreptin binds covalently to microtubule pores and lumenal taxoid binding sites. *Nature chemical biology* **3** (2), 117 (2007).

[43] Vanderwal, Christopher D., Vosburg, David A., Weiler, Sven, and Sorensen, Erik J., An Enantioselective Synthesis of FR182877 Provides a Chemical Rationalization of Its Structure and Affords Multigram Quantities of Its Direct Precursor. *J. Am. Chem. Soc.* **125** (18), 5393 (2003).

[44] Garrett M. Morris, David S. Goodsell Robert S. Halliday Ruth Huey William E. Hart Richard K. Belew Arthur J. Olson, Automated docking using a

Lamarckian genetic algorithm and an empirical binding free energy function. *Journal of Computational Chemistry* **19** (14), 1639 (1998).

45 This microtubule was developed in our group

46 Zhou, Z., Felts, A. K., Friesner, R. A., and Levy, R. M., Comparative Performance of Several Flexible Docking Programs and Scoring Functions: Enrichment Studies for a Diverse Set of Pharmaceutically Relevant Targets. *J. Chem. Inf. Model.* **47** (4), 1599 (2007).

47 Snyder, J. P., The microtubule-pore gatekeeper. *Nature chemical biology* **3** (2), 81 (2007).

48 Berman, H. M. et al., The Protein Data Bank. *Nucleic Acids Res* **28** (1), 235 (2000).

49 Progress in reducing measles mortality--worldwide, 1999-2003. *MMWR Morb Mortal Wkly Rep* **54** (8), 200 (2005).

50 Shigeta, S. et al., Antiviral activities of ribavirin, 5-ethynyl-1-beta-D-ribofuranosylimidazole-4-carboxamide, and 6'-(R)-6'-C-methylneplanocin A against several ortho- and paramyxoviruses. *Antimicrob Agents Chemother* **36** (2), 435 (1992).

51 Gabrielsen, B. et al., Synthesis and antiviral evaluation of N-carboxamidine-substituted analogues of 1-beta-D-ribofuranosyl-1,2,4-triazole-3-carboxamidine hydrochloride. *J Med Chem* **35** (17), 3231 (1992).

52 Jansen, V. A. et al., Measles outbreaks in a population with declining vaccine uptake. *Science* **301** (5634), 804 (2003).

53 Barnard, D. L., Inhibitors of measles virus. *Antivir Chem Chemother* **15** (3), 111 (2004).

54 Plemper, R. K. et al., A target site for template-based design of measles virus entry inhibitors. *Proc Natl Acad Sci U S A* **101** (15), 5628 (2004).

55 Sun, A. et al., Nonpeptide inhibitors of measles virus entry. *J Med Chem* **49** (17), 5080 (2006).

56 Sun, A. et al., Potent non-nucleoside inhibitors of the measles virus RNA-dependent RNA polymerase complex. *J Med Chem* **51** (13), 3731 (2008).

57 Hendlich, M. et al., RELIBase - an object-oriented comprehensive receptor-ligand database. *Folding Des.* **1** (Suppl.), S30 (1996); Bergner, A. et al., Use of Relibase for retrieving complex three-dimensional interaction patterns including crystallographic packing effects. *Biopolymers* **61** (2), 99 (2001).

58 Dunitz, J. D., Organic fluorine: odd man out. *Chembiochem* **5** (5), 614 (2004).

59 Zhang, Y. et al., Structural and virological studies of the stages of virus replication that are affected by antirhinovirus compounds. *Journal of virology* **78** (20), 11061 (2004).

60 Buhrman, G., de Serrano, V., and Mattos, C., Organic solvents order the dynamic switch II in Ras crystals. *Structure* **11** (7), 747 (2003).

61 Bernstein, P. R. et al., Nonpeptidic inhibitors of human leukocyte elastase. 3. Design, synthesis, X-ray crystallographic analysis, and structure-activity relationships for a series of orally active 3-amino-6-phenylpyridin-2-one trifluoromethyl ketones. *Journal of medicinal chemistry* **37** (20), 3313 (1994).

62 Smallheer, J. M. et al., SAR and factor IXa crystal structure of a dual inhibitor of factors IXa and Xa. *Bioorg Med Chem Lett* **14** (21), 5263 (2004).

63 Kurumbail, R. G. et al., Structural basis for selective inhibition of cyclooxygenase-2 by anti-inflammatory agents. *Nature* **384** (6610), 644 (1996).

64 Weber, A. et al., Unexpected nanomolar inhibition of carbonic anhydrase by COX-2-selective celecoxib: new pharmacological opportunities due to related binding site recognition. *Journal of medicinal chemistry* **47** (3), 550 (2004).